

Analysis of Three SU UMa-Type Dwarf Novae in the Kepler Field

Taichi KATO

Department of Astronomy, Kyoto University, Sakyo-ku, Kyoto 606-8502
tkato@kusastro.kyoto-u.ac.jp

and

Yoji OSAKI

Department of Astronomy, School of Science, University of Tokyo, Hongo, Tokyo 113-0033
osaki@ruby.ocn.ne.jp

(Received 201 0; accepted 201 0)

Abstract

We studied the Kepler light curves of three SU UMa-type dwarf novae. Both the background dwarf nova of KIC 4378554 and V516 Lyr showed a combination of precursor-main superoutburst, during which superhumps always developed on the fading branch of the precursor. This finding supports the thermal-tidal instability theory as the origin of the superoutburst. A superoutburst of V585 Lyr recorded by Kepler did not show a precursor outburst and the superhumps developed only after the maximum light, a first example in the Kepler data so far. Such a superoutburst is understood within the thermal-tidal instability model as a “case B” superoutburst discussed by Osaki, Meyer (2003). The observation of V585 Lyr made the first clear Kepler detection of the positive period derivative commonly seen in the “stage B” superhumps in dwarf novae with short orbital periods. In all objects, there was no strong signature of a transition to the dominating stream impact-type component of superhumps. This finding suggests that there is no strong indication of an enhanced mass-transfer following the superoutburst. In V585 Lyr, there were “mini-rebrightenings” with amplitudes of 0.2–0.4 mag and periods of 0.4–0.6 d between the superoutburst and the rebrightening. We have determined the orbital period of V516 Lyr to be 0.083999(8) d. In V516 Lyr, some of outbursts were double outbursts in a various degree. The preceding outburst in the double outburst was of the inside-out nature while the following one was of the outside-in nature. One of superoutbursts in V516 Lyr was preceded by a double precursor. The preceding precursor failed to trigger a superoutburst and the following precursor triggered a superoutburst by developing positive superhumps. We have also developed a method for reconstructing the superhump light curve and for measuring the times of maxima from poorly sampled Kepler LC data.

Key words: accretion, accretion disks — stars: dwarf novae — stars: individual (KIC 4378554, V585 Lyr, V516 Lyr) — stars: novae, cataclysmic variables

1. Introduction

Cataclysmic variables (CVs) are close binary systems consisting of a white dwarf and a mass-transferring red dwarf star. Among CVs, there are dwarf novae (DNe) which show semi-periodic outbursts with amplitudes of 2–8 mag [for a review of CVs and DNe, see e.g. Warner (1995)]. Some of the DNe, called the SU UMa sub-type, show longer and brighter outbursts called superoutburst, during which semi-periodic modulations (superhumps) having periods one-to-several percent longer than the orbital period (P_{orb}). The superhump period (P_{SH}) is believed to represent the synodic period between P_{orb} and the precession period of the non-axisymmetric (also referred to as eccentric or flexing) accretion disk. This non-axisymmetric deformation of the disk is believed to be caused by the 3:1 resonance tidal instability (Whitehurst 1988; Hirose, Osaki 1990; Lubow 1991). It is generally believed that the SU UMa-type phenomenon is a combination of the thermal instability (Osaki 1974; Meyer, Meyer-Hofmeister 1981) and tidal instability, and this is

called the thermal-tidal instability (TTI) model (Osaki 1989; see, Osaki 1996 for a review).

There have been, however, long-lasting debates whether enhanced (or modulated) mass-transfer either plays a role in producing superoutbursts or superhumps [generally called enhanced mass-transfer (EMT) model; e.g. Smak 1991; Smak 2004; Smak 2008], or an enhanced mass-transfer caused by the outburst may modify the behavior of the outburst (cf. Lasota 2001; Patterson et al. 2002), while it has been argued that an enhanced mass-transfer is difficult to occur in an irradiated secondary star in DNe (cf. Osaki, Meyer 2004; Viallet, Hameury 2007; Viallet, Hameury 2008).

By analysis of the Kepler data of V1504 Cyg, Osaki, Kato (2013a) have demonstrated that the TTI model best explains the general behavior of SU UMa-type dwarf novae, particularly the disk radius variation during the supercycle (the cycle between the successive superoutbursts) by employing the frequency of negative superhumps as a probe. The data presented in Osaki, Kato (2013a) also indicated that there is no pronounced enhanced mass-

transfer before or around the start of the superoutburst, disqualifying the EMT model as a dominant mechanism to produce superoutbursts. Furthermore, Osaki, Kato (2013a) demonstrated that the appearance of superhumps (manifestation of the tidal instability) is closely related to the development of the superoutburst, that is the development from the precursor outburst to the main superoutburst, and they concluded that the superhump and superoutburst are so much entwined that one is almost difficult to find any interpretation other than the TTI model. Osaki, Kato (2013b) further studied Kepler observations of V1504 Cyg and V344 Lyr by using a newly developed two-dimensional least absolute shrinkage and selection operator (Lasso) power spectra to strengthen the conclusion.

The situation for the enhanced mass-transfer caused by the outburst is less clear. There have been Kepler observations of V344 Lyr (Wood et al. 2011; Kato et al. 2012), which showed prominent secondary superhump maxima during the late stage of the superoutburst which smoothly developed into so-called late superhumps, which have ~ 0.5 phase shift from main superhumps (Vogt 1983). The strength of these secondary superhump maxima might suggest an enhanced mass-transfer as their origin. Since the strength of the secondary superhump was reported to be much weaker in V1504 Cyg (Kato et al. 2012), it is necessary to study whether the secondary superhump or late superhumps with ~ 0.5 phase offset are generally present in many SU UMa-type dwarf novae. The ground-based study seems to suggest that these late superhumps with ~ 0.5 phase offset are relatively rare except objects with high mass-transfer rates (\dot{M}) (Kato et al. 2012). This needs to be tested by higher-quality observations.

The presence of late superhumps with ~ 0.5 phase shift in low- \dot{M} systems are also a point of debate since a close examination of a large compilation of ground-based observations suggests that most of previously reported late superhumps with ~ 0.5 phase shift can be explained by a combination of the discontinuous decrease of the superhump period and the gap (traditional observations usually had gaps in the daytime from one observing location) in the observation (Kato et al. 2009). This interpretation also requires confirmation by uninterrupted, high-quality space observations.

NASA’s Kepler satellite (Borucki et al. 2010; Koch et al. 2010) which was aimed to detect extrasolar planets, provide the best opportunity to answer such questions. The Kepler field contains several CVs, and so far observations using the Kepler data have been reported for four SU UMa-type dwarf novae and one SS Cyg dwarf nova. They are V344 Lyr (Still et al. 2010; Cannizzo et al. 2010; Wood et al. 2011; Kato et al. 2012; Cannizzo et al. 2012; Osaki, Kato 2013b), V1504 Cyg (Kato et al. 2012; Cannizzo et al. 2012; Osaki, Kato 2013a; Osaki, Kato 2013b; Coyne et al. 2012), V516 Lyr (Garnavich et al. 2011), the background dwarf nova of KIC 4378554 (Barclay et al. 2012); and an SS Cyg-type dwarf nova with shallow eclipses — V447 Lyr (Ramsay et al. 2012). In addition to these DNe, other classes of CVs have been also studied or discovered: MV Lyr (Scaringi et al. 2012b; Scaringi et al. 2012a), KIC

8751494 (Kato, Maehara 2013) (novalike variables), KIC 4547333 (Fontaine et al. 2011) (AM CVn-type object). Kepler observations were either performed with high time-resolution (~ 1 min) mode, or short cadence (SC) runs or low time-resolution (~ 29.4 min) mode, or long cadence (LC) runs. Since the number of targets observable with SC is severely limited, most of Kepler targets were recorded with the LC mode. Some of these CVs were also recorded with the SC mode.

Although these objects are expected to play an important role in studying superhumps in detail, there are several obstacles which were not met in V1504 Cyg and V344 Lyr: faintness of the objects (V516 Lyr, the background dwarf nova of KIC 4378554), the presence of a close contaminating star (the background dwarf nova of KIC 4378554), the lack of suitable SC runs (many objects). The lack of suitable SC runs makes the analysis particularly difficult because the time-resolution of LC runs are typically a third or a fourth of the superhump period of a typical SU UMa-type dwarf nova. There is a need to develop methods to tackle these difficulties. Here, we present the results of three SU UMa-type dwarf novae using new techniques.

2. Background Dwarf Nova of KIC 4378554

2.1. Introduction and Data Analysis

This SU UMa-type dwarf nova was discovered by Barclay et al. (2012) as a background object of the Kepler target star of KIC 4378554. We analyzed the public LC Kepler data to better characterize this object.

Since the light of this object is mostly outside the aperture of the original target star KIC 4378554 (*SAP_FLUX*), we applied a custom aperture centered on this object just as in Barclay et al. (2012). Since we are mainly interested in the short-term variation (i.e. superhumps) rather than the outburst amplitudes, we did not adopt a sophisticated method described in Barclay et al. (2012). We added the observed count rates in the custom aperture and subtracted for the “sky” values estimated from the surrounding pixels just as in ordinary aperture photometry (see appendix 1 for details). Since the background is highly contaminated by the light of KIC 4378554 and the systematic background level is slowly variable (Barclay et al. 2012), we subtracted linear fits obtained from the data outside the outbursts. This procedure produces the zero count for the averaged quiescent brightness of this object. This is considered to be a good first-order approximation because this object was undetectable in Kepler full-frame image in quiescence (Barclay et al. 2012). The numbers of pixels for the custom aperture were three for Q3 and Q4, two for Q5 and Q7. For quarters in which the object was not detected in outburst, we used the apertures used in the nearest quarters (three for Q1 and Q2, two for Q8).

Since the superhump period is relatively long (~ 4 LC exposures), we simply applied the fitting method described in Kato et al. (2009) to determine the times of superhump maxima and the amplitudes as follows. We

extracted times of superhump maxima by numerically fitting a template superhump light curve around the times of observed maxima. We used a template averaged (spline interpolated) superhump light curve in GW Lib, which shows a typical asymmetric profile of superhumps in SU UMa-type dwarf novae. We used two superhump cycles (typically containing 6–8 data points) around maxima. This method worked well, and it has become evident that we do not have to pay special attention for the poor time-resolution of LC measurements in characterizing superhumps in long- P_{SH} systems.

The result for the superoutburst and its associated normal outbursts in Q3–Q4 is shown in figure 1. In order to better produce the brightness variation during outbursts, we added a constant to the flux (which was originally adjusted to be zero outside the outbursts) so that the quiescent magnitude matches the typical amplitudes (~ 5 mag) of superoutbursts in SU UMa-type dwarf novae with similar P_{SH} . Although this treatment is artificial and the global trend of variation in the faintest part is not reliable, this correction is expected to produce a better representation of the light curve when the system was in low brightness, especially the post-superoutburst stage. We could not detect the orbital period in the quiescent data. In calculating the superhump periods (figure 1, third panel), we made a linear regression to 20 adjacent times of maxima measured by template fitting. We should note that variation of the period is smoothed by this time scale (~ 1.5 d). The 1σ error is a formal error of linear regression.

2.2. System Characteristics

Although Barclay et al. (2012) quoted, with respect to this object, VW Hyi, which is a prototype SU UMa-type dwarf nova with frequent outbursts, we suggest that this object belongs to a group of objects with much low \dot{M} because typical intervals of normal outbursts (OB3 and OB4, OB4 and OB5 in Barclay et al. 2012) are an order of 200 d, and more than 200 d quiescent interval was recorded before OB1. These recurrence times are much longer than the typical recurrence times of 28 d in VW Hyi (e.g. van der Woerd, van Paradijs 1987). The long recurrence times recorded in this object is more characteristic to SU UMa-type dwarf novae with lower \dot{M} . If we assume the cycle length of normal outbursts (T_n) is proportional to \dot{M}^{-2} (cf. Ichikawa, Osaki 1994; Osaki 1996), \dot{M} in V516 Lyr is expected to be ~ 2.7 times smaller than in VW Hyi and with this \dot{M} the superoutburst recurrence time (i.e., the supercycle length) is expected to be about 500–700 d.

The sequence of outbursts shown in figure 1 is very characteristic to those of such low- \dot{M} dwarf novae: precursor outburst – main superoutburst – post-superoutburst rebrightening. Similar examples are found in many objects: the 2003 superoutburst of V699 Oph (Kato et al. 2009), the 2007 and 2009 superoutbursts of QZ Vir (Ohshima et al. 2011). Even when precursor outbursts were not present (this may have been partly due to the lack of observations before the superoutbursts), a

post-superoutburst rebrightening is frequently observed in many SU UMa-type dwarf novae (see examples in Kato et al. 2009), and the precursor outburst is also a common feature in many SU UMa-type dwarf novae (see e.g. Kato 1997; Uemura et al. 2005; Shears et al. 2011; Imada et al. 2009; Wood et al. 2011). We therefore identified the sequence of outbursts (OB1–OB3 in Barclay et al. 2012) as a complex of precursor outburst (OB1) – main superoutburst (OB2) – post-superoutburst rebrightening (OB3). The short interval between the end of OB2 and OB3, as compared to those of other normal outbursts, is then naturally understood. Post-superoutburst rebrightenings, however, are more frequently observed in shorter- P_{orb} systems (cf. Kato et al. 1998). There was a deep dip between the precursor and the main superoutburst. Such a deep dip is difficult to explain in the pure thermal instability model proposed by Cannizzo et al. (2010), because the precursor in their model just looks like a shoulder in the superoutburst light curve [cf. subsection 3.2 in Osaki, Kato 2013a].

SU UMa-type dwarf novae with P_{SH} similar to this object tend to show more frequent outbursts. There are only few moderately studied systems having comparable P_{SH} and outburst frequencies to this object. We give an example of EG Aqr [$P_{\text{SH}}=0.078828(6)$ d; Imada et al. 2008]. EG Aqr showed a superoutburst in 2006 with a small precursor and the intervals of superoutburst were 800–1000 d (Kato et al. 2013). The supercycle length of EG Aqr is similar to what is expected (~ 500 – 700 d) for this object from the cycle length of normal outbursts. QY Per [$P_{\text{SH}}=0.07861(2)$ d; Kato et al. 2009] may be another similar object, although the frequency of outbursts is lower in QY Per. The representative objects having P_{SH} similar to this object but showing less frequent outbursts, RZ Leo (Ishioaka et al. 2001) and V1251 Cyg (Kato 1995; Kato et al. 2010) do not resemble the present object in that they show intervals of several days (with double-wave modulations) before superhumps appear and in that they do not show precursor outbursts.

2.3. Development of Superhumps

The second and bottom panels of figure 1 show the development of superhumps in this system. As can be seen more clearly in the enlarged $O-C$ diagram in the second panel, there are clear three distinct stages as discussed in Kato et al. (2009): a stage with long, relatively constant superhump period ($E \lesssim 30$; stage A), a stage with a shorter period with a zero to slightly positive period derivative ($P_{\text{dot}} = \dot{P}/P$) ($30 \lesssim E \lesssim 70$; stage B) and stage with a shorter superhump period ($E \gtrsim 70$; stage C). As shown in figure 4 of Kato et al. (2009), objects with longer P_{SH} tend to have shorter duration of stage B. This tendency well matches the behavior in this object.

The transition from stage A to B, however, took place later than when the amplitude of superhumps reached a maximum. Such a finding was not recorded in the ground-based study, and it may be one of the advantages in analyzing the Kepler data. Using the epochs of superhump maxima for $0 \leq E \leq 17$, before the amplitude of the su-

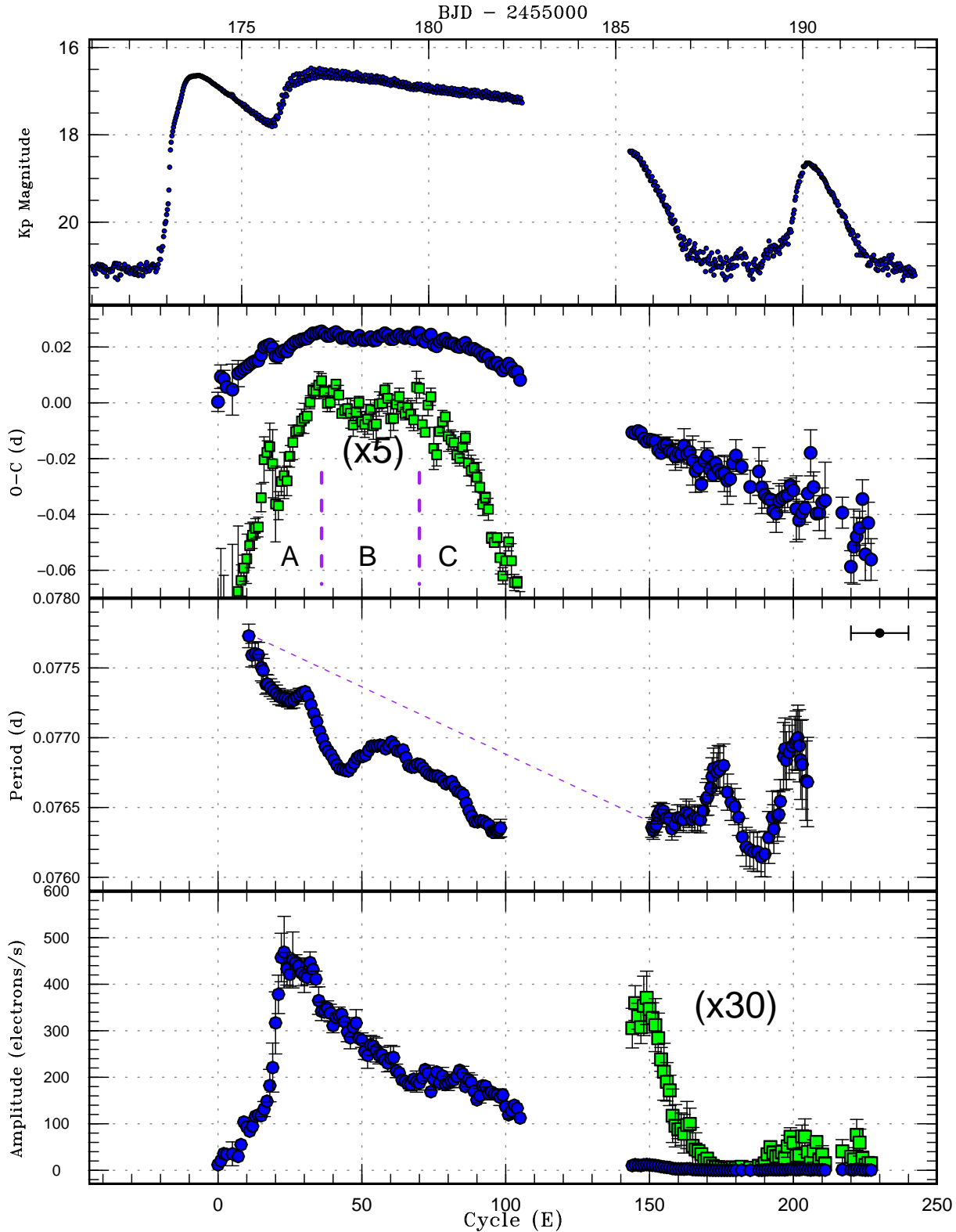


Fig. 1. Analysis of the background dwarf nova of KIC 4378554. From top to bottom: (1): Light curve. A constant was added to the flux so that the outburst amplitude matches the typical amplitudes (~ 5 mag) of superoutbursts in SU UMa-type dwarf novae with similar P_{SH} . This treatment is artificial and global trend of variation in the faintest part is not reliable. (2): $O-C$ diagram of the superhumps (filled circles). Filled squares represent $O-C$ values multiplied by five (and shifted arbitrarily by a constant) to better visualize the subtle variation during the superoutburst. An ephemeris of $\text{BJD } 2455174.368 + 0.07690E$ was used to draw this figure. (3): Period determined from the $O-C$ diagram. The period was determined by a linear regression to the adjacent 20 times of maxima (~ 1.5 d). The window width is indicated by a horizontal bar at the upper right corner. The error refers to 1σ error in this regression. Note that this process introduce artificial smoothing of the period variation and the error is only a random error which is likely smaller than the actual error. The dashed line is an imaginary global trend of the period decrease in the absence of the pressure effect assuming that the period changes linearly (will be discussed in subsection 5.2.1). (4): Amplitudes of the superhumps.

perhumps suddenly grew, we obtained a mean superhump period of 0.07781(10) d. We regarded this period to be the representative superhump period when the superhumps were growing (here we call it stage A1). The latter part of stage A (we here call it stage A2) has a mean period of 0.07727(5) d, slightly shorter than the period during stage A1.

Using the segment of $36 \leq E \leq 70$, when the $O-C$ diagram showed a positive P_{dot} , we determined the mean period of stage B superhumps as 0.07690(2) d and P_{dot} as $+13(4) \times 10^{-5}$. Using the segment $70 \leq E \leq 105$, we determined the period of stage C superhumps to be 0.07650(2) d. The period of stage C superhumps is 0.5% shorter than the mean period of stage B superhumps, in good agreement with the general behavior described in Kato et al. (2009). During stage B, the amplitude of superhumps monotonously decreased while it grew again slightly after the transition to stage C. This behavior is also similar to other systems (Kato et al. 2012). The mean profiles of superhumps on individual 1-d segments are shown in figure 2.

Although there was an unavoidable gap (a gap between Kepler quarters) after $E = 105$, the later ($E \geq 144$) development in the $O-C$ diagram when Kepler restarted observation appears to be on a smooth extension of stage C superhumps. This suggests that the period and phase of superhumps did not greatly change during the gap of the observations. By using all $E \geq 70$ times of maxima, we obtained a period of 0.07643(1) d. The object immediately entered the rapid fading stage of the superoutburst as the observation resumed. The $O-C$ curve did not show a strong variation despite the rapid brightness decline. This feature was also commonly seen in many SU UMa-type dwarf novae (e.g. Kato et al. 2009). The amplitudes of superhumps also decreased as the system faded (see also figure 3), and this makes clear difference to persisting superhumps in V344 Lyr (Wood et al. 2011; Osaki, Kato 2013b), which are supposed to arise from the accretion stream-disk interaction, corresponding to the traditional picture of late superhumps (Vogt 1983). We should note that the enhancement of the secondary hump in figure 9 of Barclay et al. (2012) corresponds to the late post-superoutburst stage (corresponding to day 189.5, where day x represents BJD 2455000+ x) in figure 3). There is some hint of the enhancement of the superhump amplitudes (measured in electrons s^{-1}) during the post-superoutburst rebrightening.

As already discussed in Kato et al. (2009) and in subsequent series of papers, the late stage (post-superoutburst) superhumps in low- \dot{M} SU UMa-type dwarf novae bear more characteristics of continuation of stage C superhumps than stream-disk interaction-type traditional late superhumps. This finding in the high sensitivity Kepler data adds another support that the mass-transfer rate is not greatly enhanced during superoutbursts [see also a discussion in Osaki, Meyer (2003)].

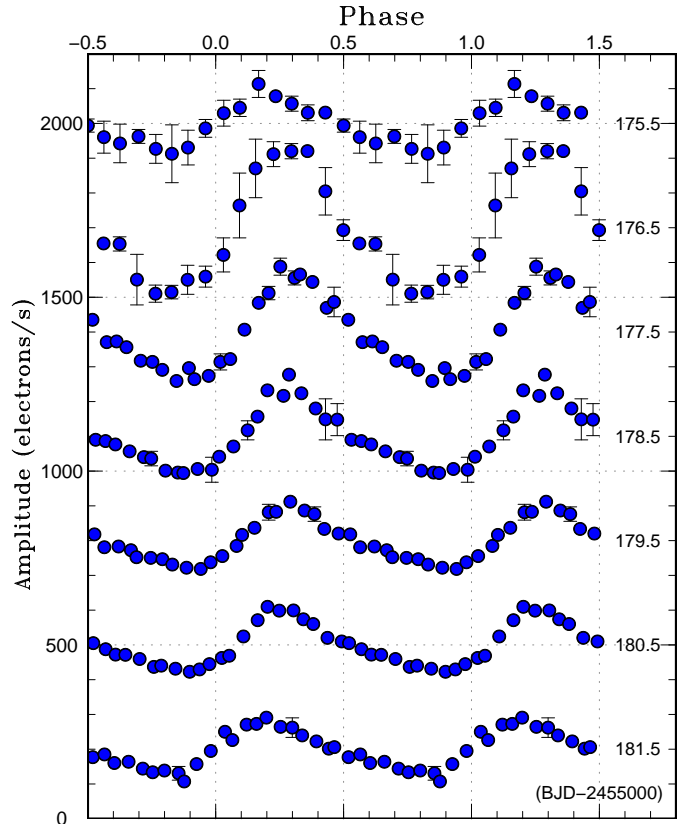


Fig. 2. Mean profiles of superhumps on individual 1-d segments during the early stage of the superoutburst of the background dwarf nova of KIC 4378554. The error bar represents a 1σ error for the average of each phase bin. The phases were calculated by an ephemeris of BJD $2455174.368 + 0.07690E$. The phases correspond to figure 1.

2.4. Oscillations before the Post-Superoutburst Rebrightening

In the light curve, there appears to be some signature of oscillations between the superoutburst and the post-superoutburst rebrightening. There are small bump-like structures around BJD 2455188.3 and 2455189.3 (the latter becomes more evident after subtracting the rising trend of the rebrightening). A trace of these features can be also seen in figure 5 of Barclay et al. (2012) and we consider that the feature is real. Since the similar feature can be better seen in V585 Lyr, we describe the characteristics in the section of V585 Lyr.

3. V585 Lyrae

3.1. Introduction and Kepler Data

V585 Lyr is a dwarf nova discovered by Kryachko (2001). Kryachko (2001) reported a long outburst and two short outbursts, and suggested that the object is an SU UMa-type dwarf nova. It is interesting that the long outburst showed a temporary fading near the start of the outburst. It was most likely accompanied by a precursor. Kato et al. (2009) studied the 2003 superoutburst and

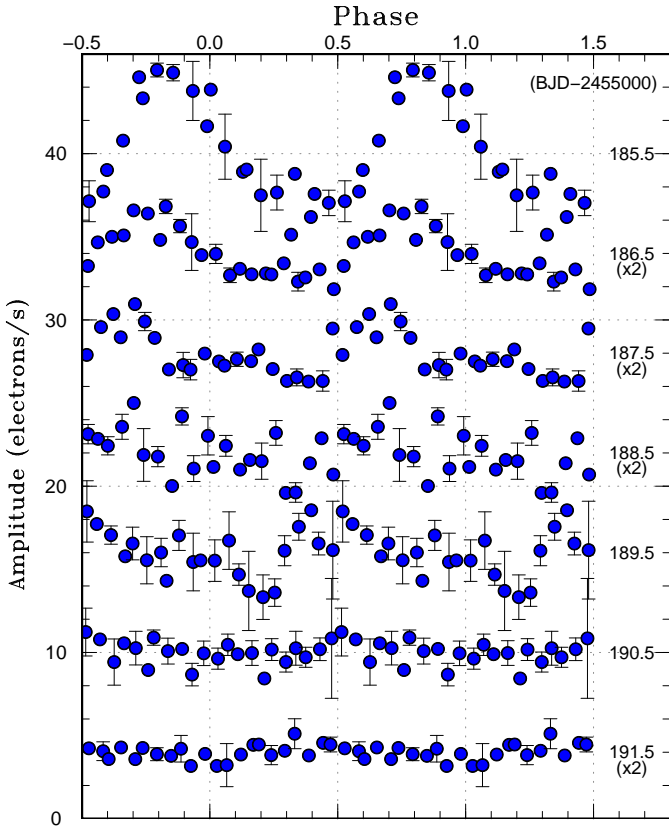


Fig. 3. Mean profiles of superhumps on individual 1-d segments during the late stage of the superoutburst, post-superoutburst and the rebrightening in the background dwarf nova of KIC 4378554. The error bar represents a 1σ error for the average of each phase bin. The phases were calculated by an ephemeris of $\text{BJD } 2455174.368 + 0.07690E$. The phases correspond to figure 1. The negative phases for the maxima are simply a result of the adoption of the constant epoch and period. The smooth variation of the phase of maxima indicates the absence of a phase shift.

Kato et al. (2013) reported on the less observed 2012 superoutburst. Howell et al. (2013) reported an unsuccessful attempt to obtain a spectrum.

The Kepler public data for V585 Lyr available in this writing are those of Q2–Q10 for LC and Q9 and Q14 for SC. V585 Lyr is sufficiently isolated from nearby stars, we used `SAP_FLUX` for SC and LC data. Within these data there was only one outburst event recorded by Kepler, a superoutburst and its post-superoutburst rebrightening, starting at the end of 2010 January and ending at the end of February. Only LC data are available during this superoutburst, and there was more than a 4-d gap immediately after the peak of the superoutburst. Due to these restrictions, the early development of the superhumps was not sufficiently recorded. We can say, however, that there was no precursor outburst and that low-amplitude modulations already appeared ~ 6 hr after the peak brightness. These modulations likely had long periods (several hours) around their appearance, but there was an indication of emerging signals (BJD 2455229.4) having a period

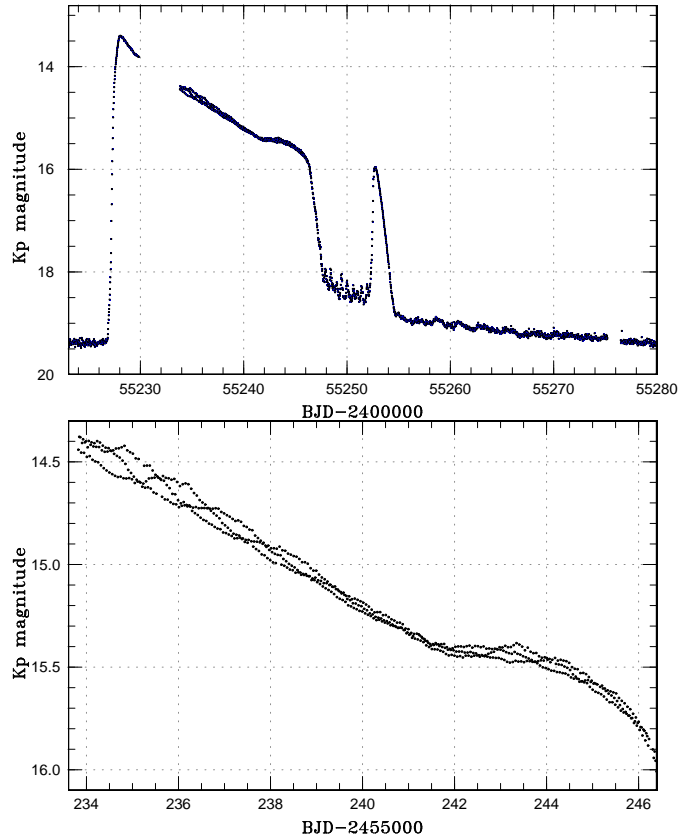


Fig. 4. The 2010 superoutburst of V585 Lyr in Kepler LC data. (Upper:) Entire outburst. (Lower:) Enlargement of the outburst to illustrate the low sampling rate of the LC data. There appear three independent curves due to the beat between the three times the LC sampling and the superhump period.

close to the superhump period, which we will discuss later. Unfortunately, the Kepler observation was stopped soon after these signal appeared. We therefore mainly focus on the analysis after the resumption of the observation at BJD 2455233.8.

The overall light curve of this superoutburst is shown in figure 4. The superoutburst started around BJD 2455227 and ended around BJD 2455248, thus its duration was about 21 d. It was followed by the post-superoutburst stage with semi-periodic variations (“mini-rebrightenings”: BJD 2455247.5–2455252; figure 5) and a distinct post-outburst rebrightening peaking at around BJD 2455252.7. The object then faded slowly with semi-periodic fluctuations with periods of ~ 2 d and amplitudes of 0.1–0.2 mag. These fluctuations almost ceased after the following 20 d (BJD 2455276).

The SC runs (Q9 and Q14) did not record any outbursts. Although the object was closely observed in quiescence in two SC runs, we could not detect any significant periodic signal for each SC run. The analysis of LC data could neither detect any signature of orbital variation.

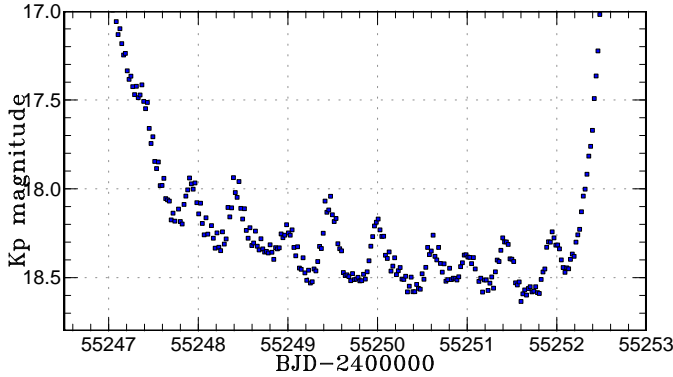


Fig. 5. The post-superoutburst stage of V585 Lyr with semi-periodic variations (“mini-rebrightenings”).

3.2. Variation of Superhump Profile from LC data

In order to obtain an $O-C$ diagram or the period variation (subsection 3.3), we need the mean profile of the superhump beforehand. We therefore first obtain the mean superhump profile and then discuss the $O-C$ variation.

As discussed below, we can see periodic light variation of superhump origin during the superoutburst of V585 Lyr with a period of about 0.060 d (or 87 min or 16.5 c/d), which is very close to three times of the LC sampling interval of 29.42 min. It is particularly difficult to obtain times of maxima or the superhump profile by conventional methods due to this low sampling rate. We therefore reconstructed the template light curves for each 0.5 d bin using the Markov-chain Monte Carlo (MCMC) modeling of the Kepler data (see appendix 2).

The result is shown in figure 6. The profile looked like double-peaked at the end of stage A (day 234.0). This feature may have been spurious since the profile was not double-peaked in the incomplete (shorter than 0.5 d) preceding bin (day 233.5). The period increased during stage B (days 234.5–242.5), and secondary humps only appeared near the end of this stage (days 241.5–242.5). The amplitudes of the superhumps grew again. Stage C with a shorter superhump period was recorded during the later stage of the superoutburst and the subsequent fading stage. The day 246.0 corresponds to the start of the rapid fading. Despite this fading, no alternation between the main and secondary humps was observed as in V344 Lyr (Wood et al. 2011). After day 247.5, the object entered the post-superoutburst stage (before the rebrightening). During this stage, mini-brightenings with periods of 0.5–0.7 d and amplitudes of ~ 0.3 mag were recorded. This phenomenon will be discussed later. The superhumps became undetectable around the peak of the rebrightening, and the waveform became difficult to trace after this rebrightening (not shown in the figure).

This result well reproduces the ground-based observations of short- P_{orb} systems such as SW UMa (Soejima et al. 2009; Kato et al. 2009) and V585 Lyr itself (Kato et al. 2009), although the ground-based observation only recorded a part of a superoutburst of V585 Lyr with lim-

ited accuracy.

3.3. $O-C$ Analysis of LC data

Using the method described in appendix 3, we determined the times of superhump maxima (figure 7). We here define $E = 0$ for BJD 2455233.8536. The result very well demonstrates the familiar stage A–B–C variations in the $O-C$ diagrams in short- P_{orb} systems [cf. Kato et al. (2009), particularly figure 3 for SW UMa ($P_{\text{orb}}=0.056815$ d)]: there was stage A with a long superhump period and with evolving superhumps ($E \lesssim 10$), stage B with the increasing superhump period ($10 \lesssim E \lesssim 140$) and stage C with a shorter, and almost constant superhump period ($E \gtrsim 140$). The mean periods for these stages were 0.06128(4) d (stage A), 0.06041(1) d (stage B) and 0.06013(1) d (stage C, limited to $140 \leq E \leq 220$). The P_{dot} for stage B was $+9.6(5) \times 10^{-5}$, which is a very characteristic value for this P_{SH} (Kato et al. 2009; Kato et al. 2010; Kato et al. 2012; Kato et al. 2013). These values very well agree the ground-based value for the 2003 superoutburst: 0.06113(8) d (stage A), 0.06036(2) d (stage B), and $P_{\text{dot}} = +10.7(12) \times 10^{-5}$ for stage B. The period of stage C superhump was not well determined in 2003 due to the short observational coverage (Kato et al. 2009). The value of 0.06035(4) d for stage B superhumps was obtained from a more sparse data set in the 2012 superoutburst (Kato et al. 2013). Although there was a possible rapid increase in the superhump period around the rising phase the rebrightening ($E \geq 290$), the reality of this phenomenon was difficult to confirm because of the signal close to the detection limit.

Independent confirmation of this pattern of period variation was obtained by two-dimensional Lasso spectrum (figure 8). This figure corresponds to figure 8 in Barclay et al. (2012), who used Fourier analysis. The frequency of the strongest (superhump) signal initially decreased (up to BJD 2455241; corresponding to stage B) and increased after then (stage B–C transition) both in the fundamental and first harmonics. This trend (i.e. initial increase and then decrease in the period) confirmed the result from the $O-C$ analysis. Note that the frequency of the first harmonics is higher than the Nyquist frequency. The Lasso analysis can handle such a case using appropriate windows and suppressing the reflected signal at the Nyquist frequency, which was seen in Barclay et al. (2012).

The $O-C$ analysis of the Kepler LC data thus perfectly confirmed the trend in short- P_{orb} systems recorded in ground-based observations. This object is the first Kepler CV showing the very distinct stages A–B–C, particularly the clear presence of stage B with an unambiguously positive P_{dot} . The Kepler observation, however, recorded the details of stage C in unprecedented quality. This observation unambiguously demonstrated the lack of phase ~ 0.5 jump (corresponding to the “traditional” late superhumps).

The variation of the superhump amplitudes was similar to those in short- P_{orb} systems recorded in ground-based observations: the peak of the superhump amplitude is close to the stage A–B transition, the amplitude

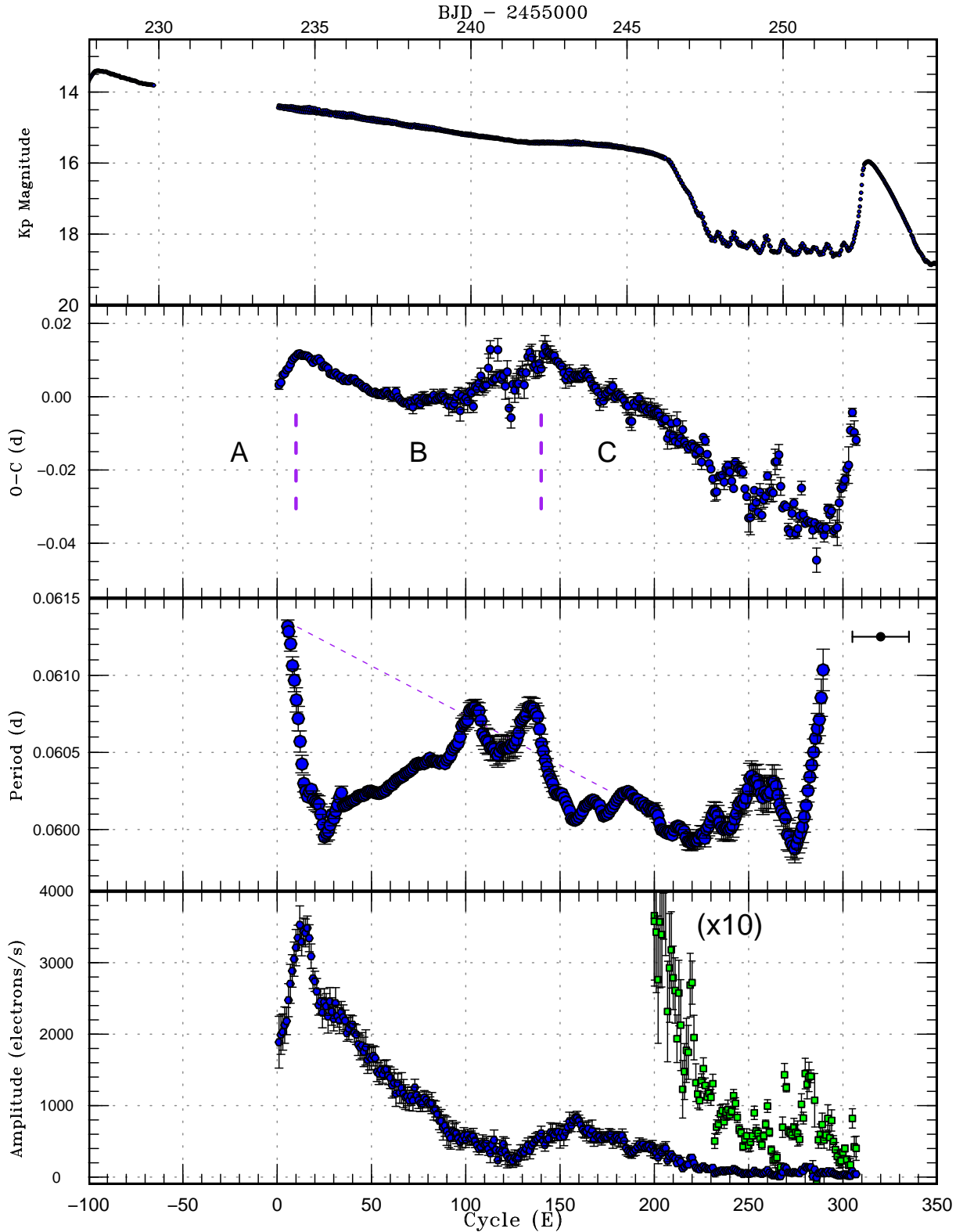


Fig. 7. $O - C$ diagram of V585 Lyr. From top to bottom: (1): Kepler LC light curve. (2): $O - C$ diagram. The figure was drawn against a period of 0.06043 d. (3): Period determined from the $O - C$ diagram. The period was determined by a linear regression to the adjacent 30 times of maxima (~ 1.8 d). The window width is indicated by a horizontal bar at the upper right corner. During stage A, 10 (~ 0.6 d) adjacent maxima were used. The error refers to 1σ error in this regression. Note that this process introduce artificial smoothing of the period variation and the error is only a random error which is likely smaller than the actual error. Wiggles (especially late stage B and stage C) were probably caused by the “beat” because the sampling rate was almost exactly one third of the superhump period, and they should not be considered as real. The dashed line is an imaginary global trend of the period decrease in the absence of the pressure effect assuming that the period changes linearly (will be discussed in subsection 5.2.1). (4): Amplitudes in electrons s^{-1} . Since modeling the Kepler data was performed by variable superhump template, the normalization of these amplitudes are not the same in different epochs. The figure is presented to show the general trend.

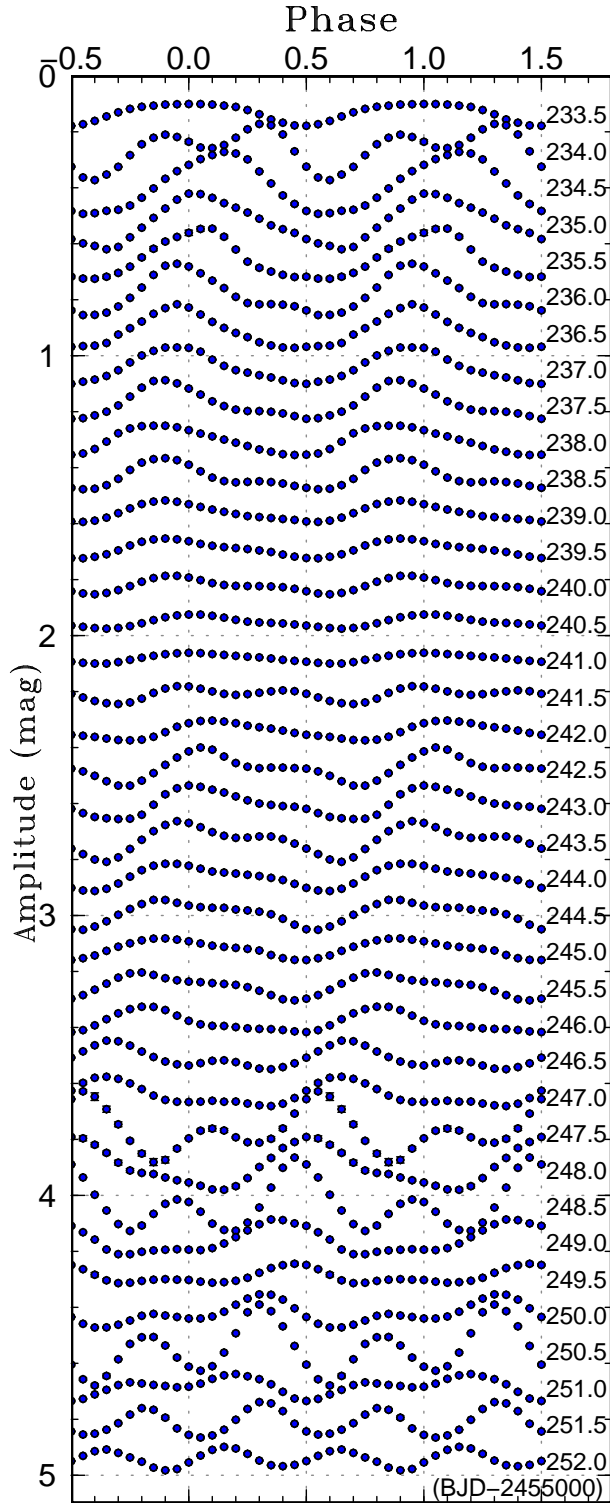


Fig. 6. Profile variation of superhumps in V585 Lyr. The profile for each 0.5-d segment of the LC data was estimated by modeling the observation (see text). The errors (smaller than figure symbols) are not true errors but numerical 1σ range of the probability distribution function. The phases were defined by an element of $\text{BJD}(\text{max}) = 2455233.7951 + 0.060437E$. The profile was double-peaked at the end of stage A (day 234.0). The period increased during stage B (days 234.5–242.5), and secondary humps only appeared near the end of this stage (days 241.5–242.5). Stage C with a shorter superhump period was recorded during the later stage of the superoutburst and the subsequent fading stage. The day 246.0 corresponds to the start of the rapid fading. Despite this fading, no alternation between the main and secondary humps was observed as in V344 Lyr (Wood et al. 2011). This figure is shown in amplitude scale for easier visibility.

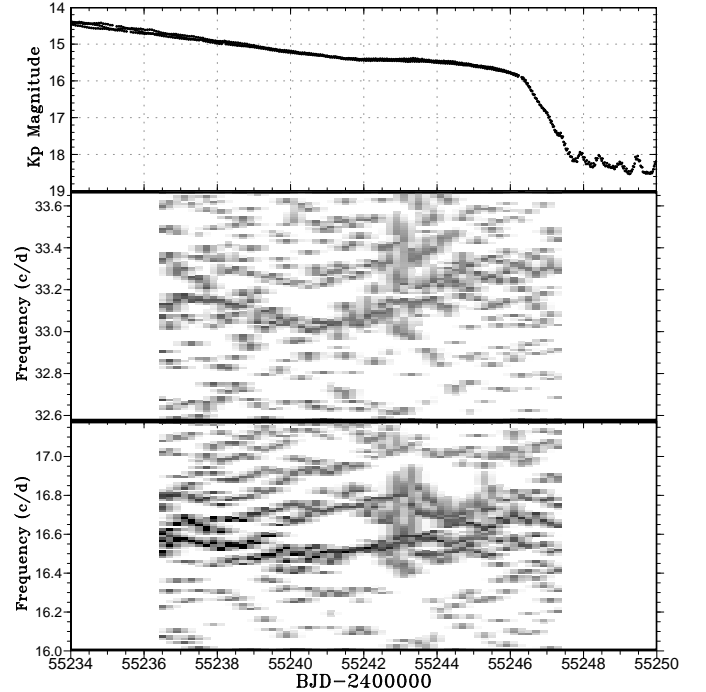


Fig. 8. Lasso analysis of superhumps of V585 Lyr in Kepler LC data. (Upper:) Light curve. (Middle:) First harmonics of the superhump signal. (Lower:) Fundamental of the superhump signal. The frequency of the strongest (superhump) signal initially decreased (up to BJD 2455241) and increased after then both in the fundamental and first harmonics. This trend confirmed the result from the $O-C$ analysis. Note that the frequency of the first harmonics is higher than the Nyquist frequency, and the Lasso analysis can detect such a signal using appropriate windows. $\log \lambda = -5.3$ was used. The width of the sliding window and the time step used are 5 d and 0.2 d, respectively.

decreases during stage B and reaches a minimum before stage B–C transition, and again increases near the stage B–C transition (Kato et al. 2012). In conjunction with the amplitude increase near the stage B–C transition, the brightness of the system also shows an upward (brighter) deviation from the linear fading. This brightening trend is commonly seen in short- P_{orb} systems (Kato et al. 2003).

3.4. Mini-rebrightenings

Between the superoutburst and the distinct post-superoutburst rebrightening (BJD 2455247.5–2455252; figure 5), there were “mini-rebrightenings” with amplitudes of 0.2–0.4 mag and periods of 0.4–0.6 d. As far as we know, such variations have never been documented before. The amplitudes appears to be too large to be explained by a beat between some period and another (e.g. between the superhump period and another period), and the periods of 0.4–0.6 d appear to be too short to be explained by a beat phenomenon. We thus regard them as real brightness variation with these time-scales. There was a hint of the same phenomenon on the declining branch from the superoutburst (BJD 2455247.4). This phenomenon disap-

peared as the object experienced the distinct rebrightening peaking at BJD 2455252.7, and never appeared again after the fading from the rebrightening.

Although this phenomenon appears to be physically related to the appearance of the post-superoutburst rebrightenings, and potentially important to understand the origin of the rebrightening, we still do not have a physical explanation for this phenomenon. Not all SU UMa-type dwarf novae show post-superoutburst rebrightenings (Kato et al. 2009), and a systematic search for such variations might lead to a solution.

As we have already seen, the background dwarf nova of KIC 4378554 also possibly showed the same phenomenon (subsection 2.4), such a phenomenon may be more prevalent and will deserve a further study.

4. V516 Lyrae

4.1. Introduction

V516 Lyr was originally identified as a blue object (NGC 6791 B8) in the region of an old open cluster NGC 6791 (Kaluzny, Udalski 1992). Kaluzny, Rucinski (1995) suspected that the object is likely a cataclysmic variable based on the color and variability. The DN-type nature was confirmed by photometry and spectroscopy by Kaluzny et al. (1997). Ground-base observations indicated that this object showed ~ 2 mag outbursts outside the $V = 21$ quiescence and was suggested to be an SS Cyg-type dwarf nova (Mochejska et al. 2003). Garnavich et al. (2011) reported from Kepler SC data that this object underwent a superoutburst on 2011 October 13 and determined the superhump period of 2.097(3) hr (in average) or 2.109(3) hr (initial two days) (Garnavich et al. 2011). Howell et al. (2013) presented a spectrum in agreement with the dwarf nova-type classification and also presented Kepler light curves showing normal outbursts with the ~ 18 d recurrence time. Howell et al. (2013)¹ also reported the possible detection of a periodicity of 0.087478 d by the LC data in the quiescent interval around BJD 2455468.

4.2. Global Light Curve

We first examine the LC Kepler light curves of V516 Lyr available for public at the present writing. They are those of Q6–Q10 and Q14. Figure 9 illustrates the Kepler light curve of the LC data of V516 Lyr for periods of Q6–10 and Q14. Since there is no long-term stable zero-point in the Kepler light curve, we artificially added constants to adjust the quiescent level to be ~ 21 mag, as recorded in Mochejska et al. (2003). As seen from figure 9, V516 Lyr exhibited about 40 outbursts including two superoutbursts in a time scale of about one and a half years. We summarize the main characteristics of these outbursts in table 1. The first column of the table is a sequential number of outbursts within a given quarter. The second and third columns are the dates of the start and the end of an outburst (determined by eye), respectively, where dates

are counted from BJD 2455000. The fourth column is the outburst duration and the fifth column gives the outburst type. The sixth column gives the duration of quiescence preceding to a given outburst and the last column is just comments, if there are any.

As discussed by Smak (1984), two types of normal outbursts are recognized; Type A outburst or the “outside-in” outburst in which the heating transition of the thermal instability starts from the outer-part of the disk and the heating front propagates inward and Type B outburst or the “inside-out” outburst in which the heating transition does in the inner-part of the disk and the heating wave propagates outward. The light curve of the Type A outburst is characterized by a rapid rise to outburst maximum as compared to the slower decay from maximum while the type B outburst is characterized by more or less symmetrical rise and fall around maximum. The judgement of outburst types is made by eye and we must admit there are some delicate and ambiguous cases in this judgement.

Two superoutbursts are seen in our data, which occurred around BJD 2455600 (SO No. 1) and 2455785 (SO No. 2). Thus the length of supercycle between these two superoutbursts is about 185 d. However, since the starting date of observations in Q6 was BJD 2455372 and since no superoutburst was apparently missed before the SO No. 1, the length of the previous supercycle must be longer than 220 d at least. The next superoutburst is expected to have occurred most likely in the period of Q12 but so far we have no way to confirm or disprove.

As discussed in the next subsection, a possible orbital period of V516 Lyr was found to be 0.0840 d (2.016 hr or 11.9 c/d) which is very near to that of V344 Lyr. However the recurrence cycles of both the normal outburst and the superoutburst suggest that V516 Lyr has slightly lower mass-transfer rate than that of V344 Lyr.

One of the most interesting characteristics in the light curve of V516 Cyg was an occurrence of several double outbursts; their examples are outbursts Q6-1, Q6-2, Q6-3, Q9-6, Q14-4, and Q14-8. The two outbursts of Q14-6 and Q14-7 are most likely a double outburst with a just one day quiescence interval. The degree of doubling varies from outburst to outburst, such as an outburst with a shoulder (e.g., Q6-3) to an outburst with a deep dip almost touching quiescence (e.g., Q14-4). As seen in figure 9, the preceding outburst in the double outburst was always type B (“inside-out”) outburst while the following one was type A (“outside-in”) outburst and there is no exception to this rule so far. The double outbursts tended to occur in group, e.g., in Q6 and Q14.

This phenomenon is understood in the following way. As mentioned above the preceding outburst is the inside-out outburst in which the heating transition first occurs in the inner part and the heating front propagates outward. But the heating front fails to reach the outer edge of the disk but is reflected in the middle of the disk (i.e., type Bb outburst in Smak’s classification). This creates a special situation in which the thermal instability is easily triggered in the outer part of the disk because a large amount

¹ In Howell et al. (2013), V516 Lyr actually refers to V523 Lyr and V523 Lyr actually refers to V516 Lyr. Their figure 4 actually shows the lightcurve of V516 Lyr, not V523 Lyr.

Table 1. Properties of outbursts of V516 Lyr.

No.	start*	end*	d_{out}^{\dagger}	type [‡]	d_{qui}^{\S}	C
Q6-1	377	381.6	4.6	double	–	
Q6-2	402.6	407.5	4.9	double	21	
Q6-3	424	428.4	4.4	shoulder	16.5	
Q6-4	437.5	440.8	3.3	A	9.1	
Q6-5	456	460	4	A	15.2	
Q7-1	472	475	3	A	12	
Q7-2	492.5	496	3.5	?	17.5	1
Q7-3	513.4	516.8	3.4	A	17.4	
Q7-4	532.8	536	3.2	A	16	
Q8-1	592.4	606.8	14.4	SO	56?	1
Q8-2	608	610.5	2.5	RB	1.2	
Q8-3	614.4	616	1.6	mini	3.9	
Q8-4	626.1	628.5	2.4	A	10.1	
Q9-1	642.9	645	2.1	B	14.4	1
Q9-2	654.8	657.8	3	B?	9.8	2
Q9-3	669.5	673.1	3.6	B	11.7	
Q9-4	684.8	688.2	3.4	B	11.7	
Q9-5	698.8	701.1	2.3	A	10.6	
Q9-6	713.4	719	5.6	double	12.3	
Q9-7	725.8	729	3.2	B	6.8	
Q9-8	736	–	–	B	–	
Q10-1	746.3	749.9	3.6	A?	–	
Q10-2	756.7	760	3.3	B	6.8	
Q10-3	766.2	769.2	3	A	6.2	
Q10-4	777.5	782.2	4.7	double	PC	
Q10-5	782.2	794	11.8	SO	0	
Q10-6	794	796.7	2.7	RB	0	
Q10-7	799.4	802	2.6	A	2.7	
Q10-8	811.3	814.8	3.5	A	9.3	
Q10-9	825	828	3	A	10.2	
Q14-1	1114.6	1117.9	3.3	B	–	
Q14-2	1134.1	1137.4	3.3	B	16.2	
Q14-3	1143.4	1146.6	3.2	B	6	
Q14-4	1155	1161	6	double	8.4	
Q14-5	1167.4	1170	2.6	mini	6.4	
Q14-6	1177	1181.3	4.3	B	7	
Q14-7	1182.3	1185.8	3.5	A	1	
Q14-8	1199.5	–	–	double?	13.7	

*BJD–2455000.

†Outburst duration (d).

‡Abbreviations: precursor (PC), rebrightening (RB), superoutburst (SO).

§Quiescence duration prior to the outburst (d).

||Comment. 1: data gap 2: too noisy.

of matter pushed outward by the heating front is left over in the outer-part by reflection (see, Cannizzo 1993). The second thermal instability in the outer part of the disk is then triggered (type A outburst) before the cooling wave of the preceding thermal instability completely reached the inner edge of the disk. The behavior of the double outburst can be well explained in the framework of the thermal disk instability.

4.3. SC Data

The object was observed in Kepler SC in Q8–Q11 and Q14. Since the object is faint in quiescence (~ 30 electrons s^{-1}) and the baseline showed systematic trends, we adjusted the quiescent level to $Kp = 21$ (as in the LC data) by subtracting low-order (up to second) polynomials to the observed count rates for each continuous quarter (duration 67–97 d). The resultant quiescent magnitudes are not real, but this treatment is sufficient since our interest is in the residual pulsed flux. The mean superhump waveform during one of its superoutburst (SO No.2 or Q10-5) is shown in figure 10. We also analyzed the SC data after excluding two superoutbursts and the post-superoutburst phase until the next normal outburst (but not excluding other normal outbursts), i.e. a combined data before BJD 2455592, BJD 2455612–2455777 and after BJD 2455805 (figure 11). The only detected signal was 0.083999(8) d, which is most likely the orbital period. We could not confirm a period of 0.087478 d reported in Howell et al. (2013). There was no hint of persisting negative superhumps or positive superhumps in quiescence in this interval. The fractional superhump excess is 4.0%, typical for this orbital period.

As in V1504 Cyg and V344 Lyr (Osaki, Kato 2013b), we calculated Fourier and Lasso two-dimensional power spectra (Kato, Uemura 2012; Kato, Maehara 2013) (figures 12, 13). Due to the faintness of the object, the power spectra are not as clear as in V1504 Cyg and V344 Lyr, particularly around quiescence. During Q8–Q11, the object underwent a relatively regular pattern of normal outburst and two superoutbursts separated by ~ 185 d. The characteristic signals of positive superhumps during superoutbursts showed an increase of the frequency (shortening of the superhump period) as reported by Garnavich et al. (2011). The orbital signal was also sometimes detected in the Lasso power spectra, but was not clearly seen in the Fourier power spectra.

Although there were no clear persistent negative superhumps as observed in V344 Lyr and V1504 Cyg, there were several occasions of impulsive (failed) negative superhumps, which are negative superhumps transiently seen during some normal outbursts [terminology introduced in Osaki, Kato (2013b); see also the description of the phenomenon in Wood et al. (2011)]. These impulsive negative superhumps occurred around BJD 2455735 (outburst Q9-8) and 2455750 (Q10-1), four and three cycles before a superoutburst.

4.4. Superoutburst with Double Precursor

The most notable feature in V516 Lyr is a “double precursor” in SO No. 2, i.e. Q10-4. Here we discuss two different possibilities for the origin of this double precursor.

The one of possible explanations is an explanation same as that of the double outburst presented in 4.2. As already discussed there, the preceding outburst is an inside-out outburst in which the heating wave is reflected in the middle of the disk. As discussed in subsection 3.2 in Osaki,

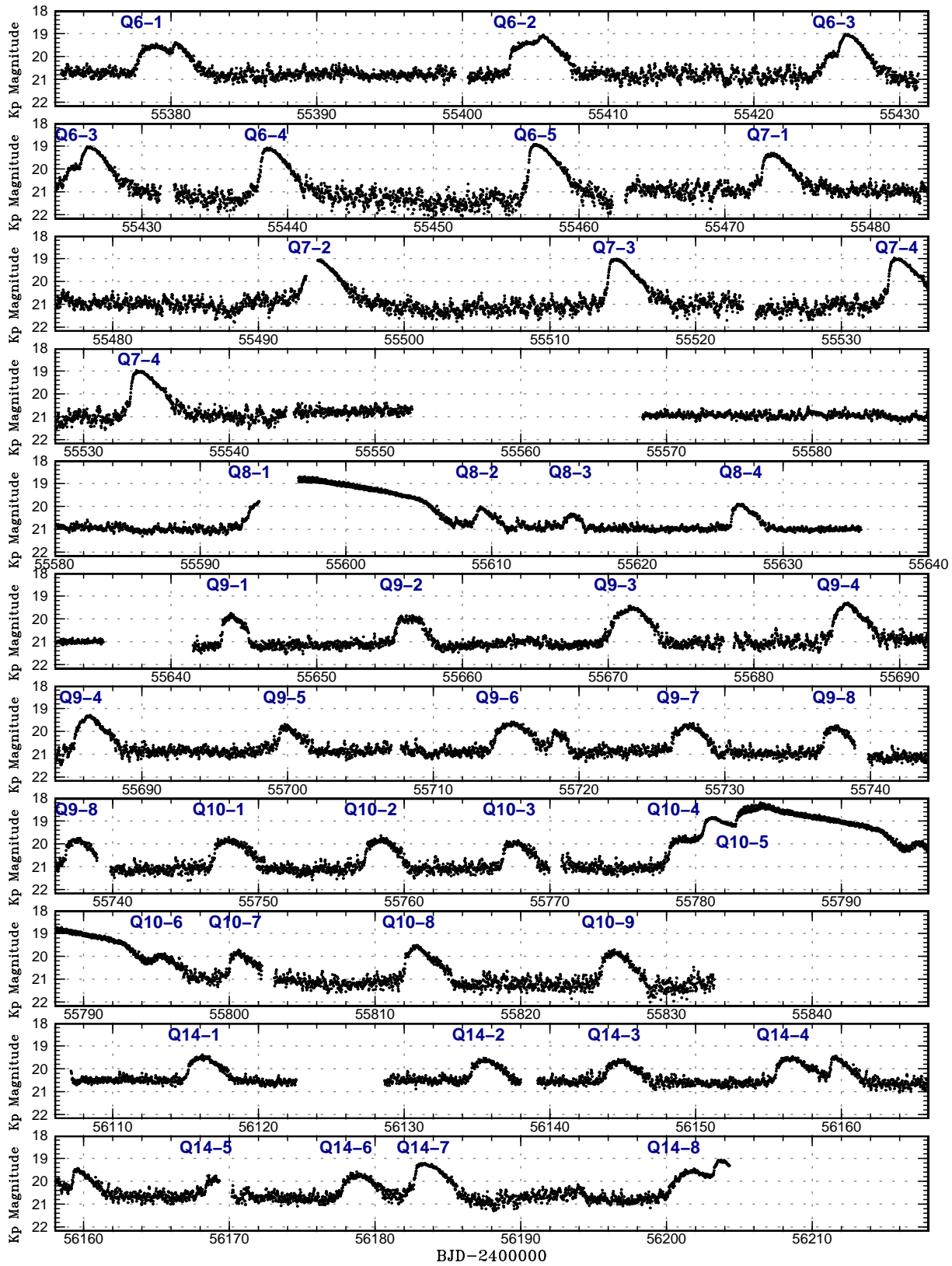


Fig. 9. The Kepler LC light curve of V516 Lyr. The numbers of the outbursts correspond to table 1.

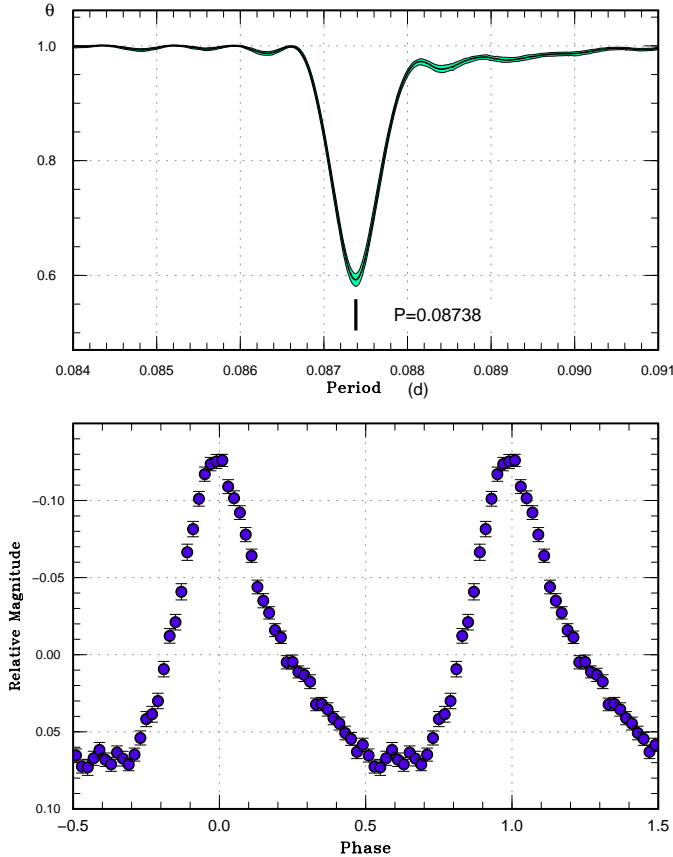


Fig. 10. Superhumps in V516 Lyr. The figure is produced as in the same way in Kato et al. (2012) for the SC data for BJD 2455783–2455793. (Upper:) Phase dispersion minimization (PDM; Stellingwerf 1978) analysis. (Lower:) Phase-averaged profile.

Kato (2013a), this type of outburst is not accompanied with the disk expansion and so it does not trigger the 3:1 resonance tidal instability. On the other hand, since the following outburst is an outside-in outburst, it is accompanied with the disk expansion and thus it can trigger the 3:1 eccentric tidal instability and it can start superhumps and a superoutburst.

Another possibility is that related to the failed precursor due to an appearance of impulsive negative superhumps. During the preceding precursor (BJD 2455778), negative superhumps seemed to have appeared [period for BJD 2455778–2445780 was 0.0828(3) d with the PDM method; figure 14]. However, this signal diminished during the following precursor and instead positive superhumps appeared just as in ordinary precursor outbursts of V344 Lyr and V1504 Cyg. In this interpretation, the preceding precursor outburst triggered the development of impulsive negative superhumps which were unable to sustain the disk in a hot state, while the second precursor successfully triggered the development of eccentric instability to produce positive superhumps and succeeded in starting a superoutburst. This kind of “failed superoutburst” due to the impulsive negative superhumps was also

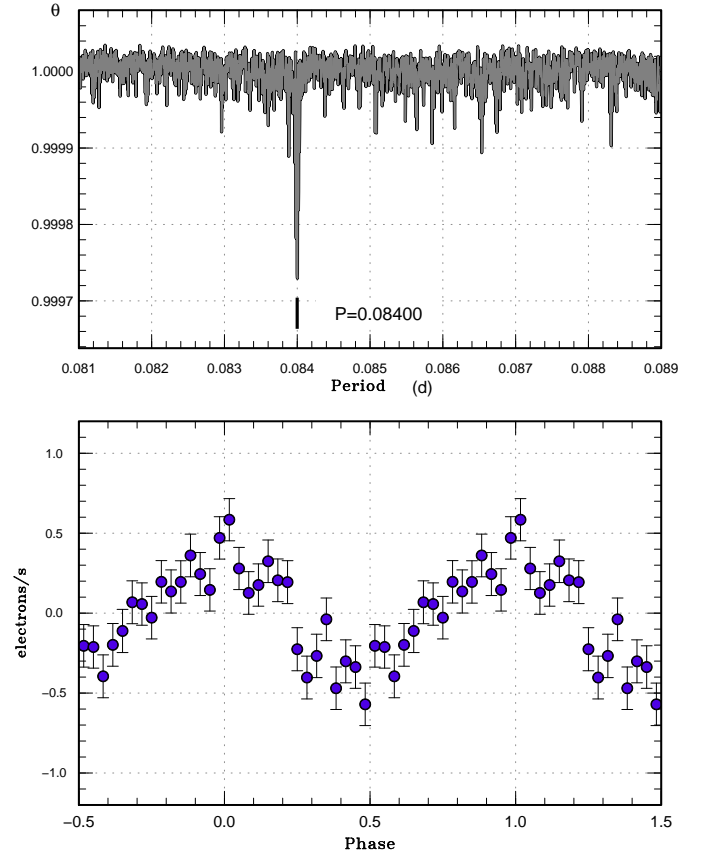


Fig. 11. Orbital signal in V516 Lyr. The SC data excluding two superoutbursts and the interval until the next normal outbursts were used. There were apparently no period other than the orbital period. (Upper:) PDM analysis. (Lower:) Phase-averaged profile.

seen in V1504 Cyg (section 4.5.2 and figure 77 in Kato et al. 2012). It is interesting to note that this failed superoutburst in V1504 Cyg occurred in the second normal outburst prior to a following superoutburst [cf. subsection 2.7 in Osaki, Kato (2013b)].

The two explanations presented above seem to contradict with each other because the inside-out type precursor with Smak’s type Bb in the first explanation is not expected to excite impulsive negative superhumps. This is because the disk does not expand with this type of outburst. Although this may contradict with observed impulsive negative superhumps, we would like to keep both explanations as possibility at this moment, since the amplitudes of the seeming impulsive negative superhumps were close to the detection limit and it is difficult to make a definite conclusion.

We note, however, there have been at least two objects which showed inside-out-type rise in the superoutburst: ER UMa (Ohshima et al. 2012) and BZ UMa (fig 150 in Kato et al. 2009). In figure 2 in Ohshima et al. (2012) for ER UMa, the transition from negative to positive superhumps took place ~ 2 d after the start of the superoutburst with a kink in the light curve. This case causes no prob-

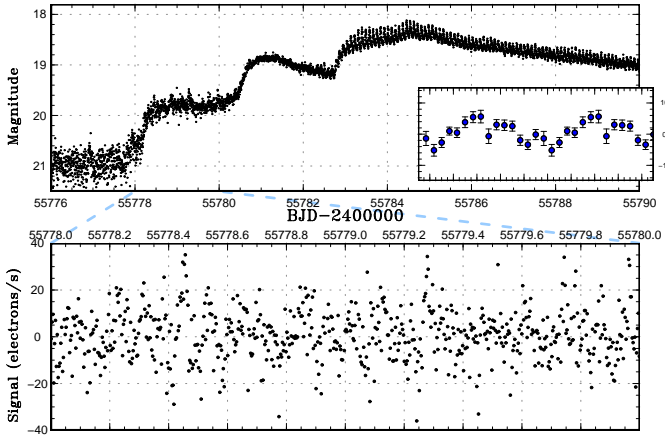


Fig. 14. Possible Impulsive negative superhumps during the double precursor. (Upper:) Kepler SC light curve (binned to 0.003 d). (Middle:) Pulsed flux (binned to 0.006 d). The inset on right edge the upper panel is the profile of impulsive negative superhumps averaged for BJD 2455778.2–2455780.0 (period=0.0828 d).

lem as an expansion of the disk occurs if the inside-out outburst is Smak’s type Ba in which the heating front propagating outward reaches the outer edge of the disk. In BZ UMa, there appears to be a weak second precursor at around BJD 2454203, after which superhumps developed, although a double-nature of the precursor is not as evident as in V516 Lyr. This superoutburst appeared to be understood as an inside-out-type precursor followed by an outside-in type second precursor, which were not well resolved from the initial precursor.

4.5. $O - C$ Analysis of Superhumps

We calculated the $O - C$ diagram of the superoutburst around BJD 2455780–2455797 (the superoutburst with double precursors). The $O - C$ diagram was roughly composed of stages A–B–C, as described in Kato et al. (2009). The transitions from stage A to B and stage B to C were rather smooth compared to short- P_{orb} systems described in Kato et al. (2009), and more resembles the long- P_{orb} , high- \dot{M} system V344 Lyr (Kato et al. 2012). Although it is not very clear what segments in E are most adequate to determine the period in each stage, we adopted periods of 0.08732(3) d and 0.08725(3) d for stage B ($38 \leq E \leq 70$) and stage C ($70 \leq E \leq 120$), respectively. During stage B, a period increase at $P_{\text{dot}} = +27(7) \times 10^{-5}$ was recorded.

There was a break in the $O - C$ diagram around the time when the amplitude of the superhump reached a maximum. As in the background dwarf nova of KIC 4378554, we refer to these stages as A1 ($E \leq 15$) and A2 ($16 \leq E \leq 38$). The mean periods of superhumps during stages A1 and A2 were 0.0894(4) d and 0.08814(3) d, 6.4(5)% and 4.93(4)% longer than the orbital period, respectively.

The profile of the superhumps (figure 16) did not show the strong secondary peak as seen in V344 Lyr (Wood et al. 2011; Kato et al. 2012). There was no clear transi-

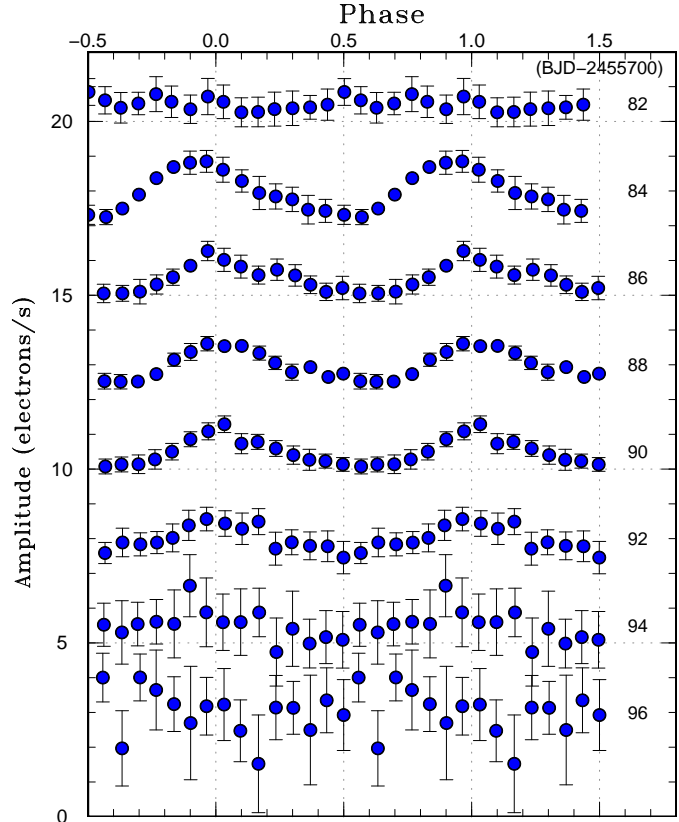


Fig. 16. Variation of superhump profiles of V516 Lyr. The phase-averaged profiles were calculated for 2-d segments. The phases were calculated using the same ephemeris as in figure 15.

tion to traditional late superhumps having a ~ 0.5 phase jump. During the late stage of the superoutburst, the amplitudes of the superhumps (including the secondary maxima, if they existed) decreased to an undetectable limit (amplitude $\lesssim 1$ electrons s^{-1}). These amplitudes were no larger than that of the orbital variations in quiescence (subsection 4.3).

4.6. LC Data

We also made a two-dimensional Lasso power spectrum of the LC data (figure 17). Since the number of data points was much smaller than in the SC data, we could only detect relatively persistent signals. The faintness of V516 Lyr also made the analysis more difficult than in V344 Lyr or V1504 Cyg (Osaki, Kato 2013b). We adopted a window of 30 d, which was shown to give the best signal-to-noise for the orbital modulation, and hence is expected to detect signals with similar strengths. This length of the window was too long to resolve any variation of positive superhumps during the superoutbursts, and these positive superhumps were only detected as broad bands. In figure 17, however, there seem to be transient weak signals of possible negative superhumps around the frequencies 12.32–12.35 c/d in segments BJD 2455500–2455560 (this may also be extended to a possible frequency 12.30

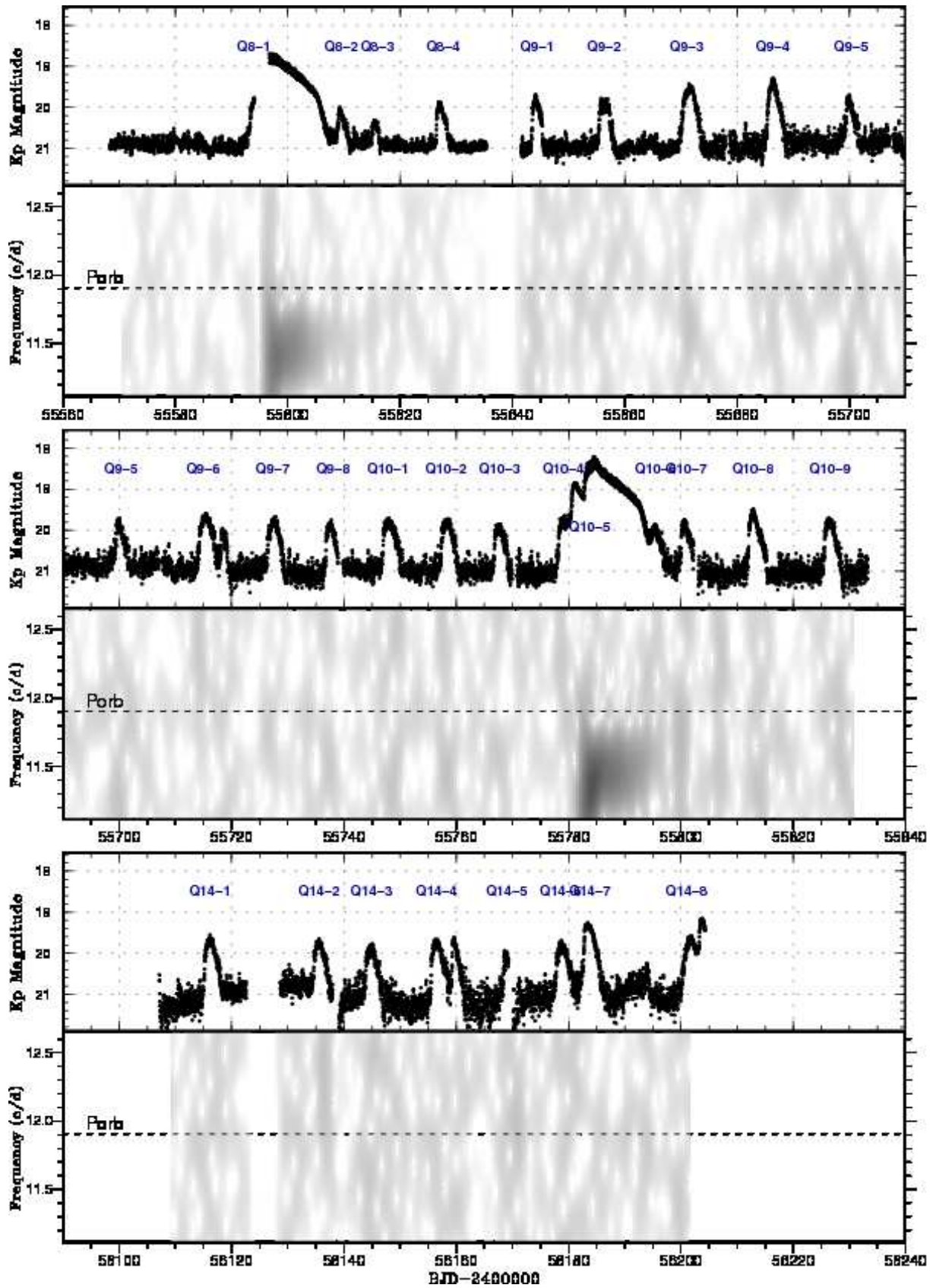


Fig. 12. Two-dimensional Fourier power spectrum of the Kepler SC light curve of V516 Lyr. (upper:) Light curve; the Kepler data were binned to 0.02 d. (lower:) Fourier power spectrum. The width of the moving window and the time step used are 5 d and 0.5 d, respectively.

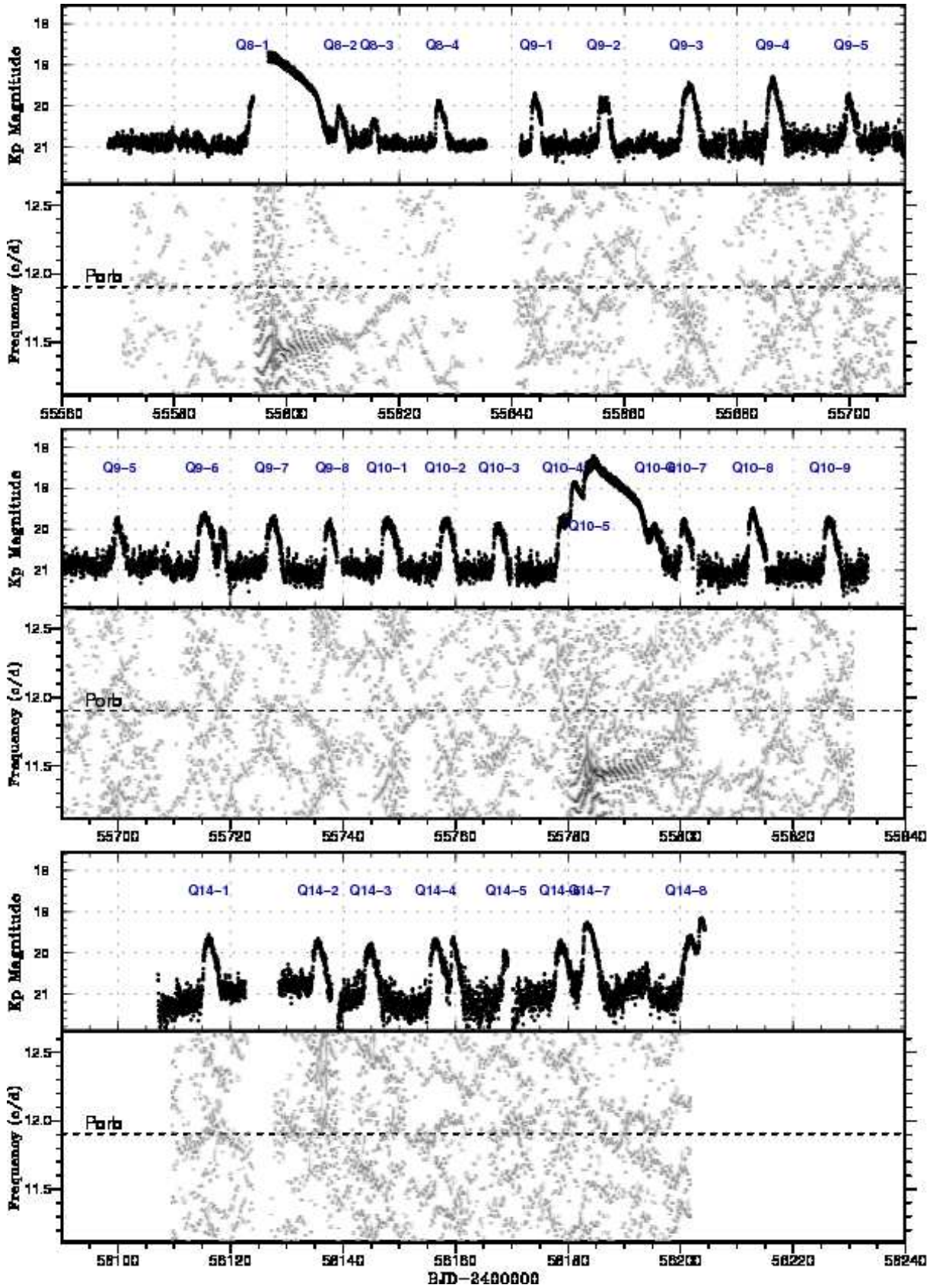


Fig. 13. Two-dimensional Lasso power spectrum of the Kepler SC light curve of V516 Lyr. (upper:) Light curve; the Kepler data were binned to 0.02 d. (lower:) Lasso power spectrum ($\log \lambda = -5.7$). The width of the moving window and the time step used are 5 d and 0.5 d, respectively.

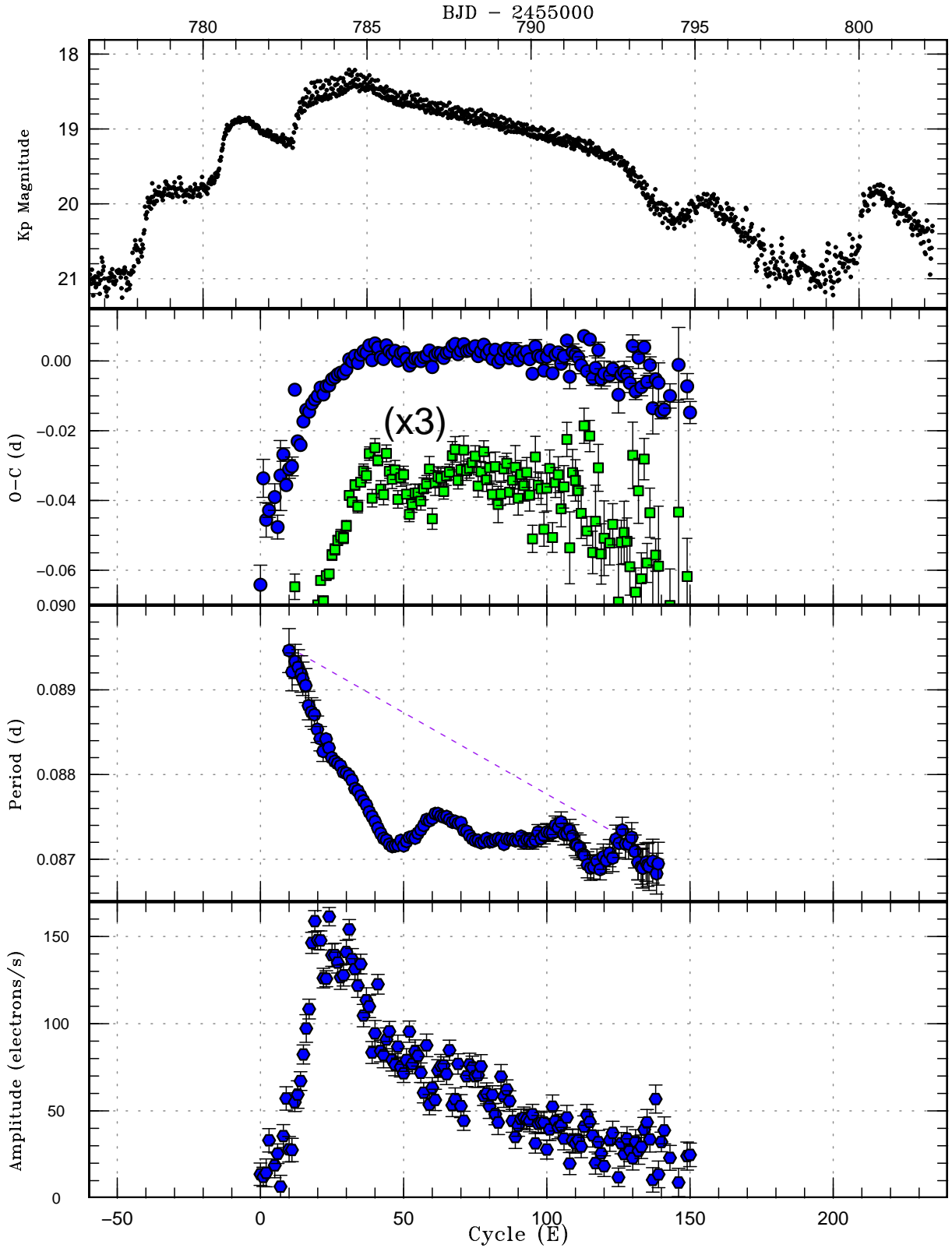


Fig. 15. Analysis of the superoutburst (BJD 2455780–2455797) in V516 Lyr. From top to bottom: (1): Light curve. The quiescent flux level was artificially adjusted to $K_p = 21$ level. Note that the magnitudes in the faintest part are not reliable. (2): $O - C$ diagram of the superhumps (filled circles). Filled squares represent $O - C$ values multiplied by three (and shifted arbitrarily by a constant) to better visualize the subtle variation during the superoutburst. A ephemeris of $\text{BJD } 2455781.750 + 0.08732E$ was used to draw this figure. (3): Period determined from the $O - C$ diagram. The period was determined by a linear regression to the adjacent 20 times of maxima (~ 1.5 d). The window width is indicated by a horizontal bar at the upper right corner. The error refers to 1σ error in this regression. Note that this process introduce artificial smoothing of the period variation and the error is only a random error which is likely smaller than the actual error. The dashed line is an imaginary global trend of the period decrease in the absence of the pressure effect assuming that the period changes linearly (will be discussed in subsection 5.2.1). (4): Amplitudes of the superhumps.

c/d around BJD 2455420–2455450), 2455730–2455760 and 2456120–2456150. Although the reality of these signals is difficult to confirm, we suspect that they were likely present because the initial segment corresponds to a period of decreased frequency of outbursts (type “L” in Osaki, Kato 2013a, and the second segment corresponds to a period of impulsive negative superhumps discussed in subsection 4.3. The ϵ^* for these possible negative superhumps was 3.5–3.7%.

Although the result is not very conclusive, the tendency that negative superhumps suppress the occurrence of outbursts (Ohshima et al. 2012; Osaki, Kato 2013a; Zemko et al. 2013) seems to be valid for V516 Lyr. If the signals around BJD 2455420–2455450 were also indeed of negative superhumps, there was an increase of the frequency of negative superhumps as the phase of the supercycle progresses, which has been confirmed in V1504 Cyg and V344 Lyr (Osaki, Kato 2013a; Osaki, Kato 2013b). We expect future Kepler SC runs (if available) during a state with negative superhumps will provide us better characterization of the phenomena. The Kepler results up to now appears to suggest that negative superhumps in quiescent SU UMa-type dwarf novae are more prevalent than have been considered.

An additional feature in the two-dimensional power spectrum analysis is that the orbital signal was more strongly detected in Q14 than in other quarters. Such a variation of the strength of the orbital signal was also seen in V1504 Cyg and V344 Lyr (Osaki, Kato 2013a; Osaki, Kato 2013b).

4.7. Interpretation of Historical Data

Although Mochejska et al. (2003) suggested the SS Cyg-type classification, it has now become evident that this object is an SU UMa-type dwarf nova. We reexamined the material in Mochejska et al. (2003). The phased light curve (figure 6) in Mochejska et al. (2003) indicated a mean period of 17.7298 d, which appears to be consistent with the Kepler observations. Their long-term light curve (figure 6, object B8) showed at least six major outbursts most of which reached maxima of $V = 19$. One of them (in their window No. 12) lasted at least 5 d, and this outburst must have been a superoutburst. On one occasion (in their window No. 3), the object was detected as faint as $V = 22 \sim 23$, more than 1 mag fainter than its ordinary quiescence. Since this object is not eclipsing, this phenomenon may have been caused by a temporary reduction of the mass-transfer rate. It is difficult to check whether a similar phenomenon was recorded in the Kepler data due to the faintness of the object and the highly variable zero-point.

5. Discussion

5.1. Appearance of Superhumps and its Implication to the Thermal-Tidal Instability Theory

In the background dwarf nova of KIC 4378554 and V516 Lyr, all superoutbursts took a form of the precursor–superoutburst combination, same as reported in V1504

Cyg and V344 Lyr (Still et al. 2010; Wood et al. 2011; Cannizzo et al. 2010; Cannizzo et al. 2012; Osaki, Kato 2013a; Osaki, Kato 2013b). In both systems, superhumps always started to appear during the fading branch of precursor and reached the maximum amplitude around the peak of the main superoutburst. This sequence of a precursor — development of superhumps — main superoutburst very well fits the picture of the TTI model (Osaki 1989; Osaki, Kato 2013a; Osaki, Kato 2013b) and strengthens the universal application of the TTI theory to two more additional SU UMa-type dwarf novae.

In the case of V585 Lyr, the superhump took ~ 7 d to reach the maximum amplitude. This long waiting time compared to the background dwarf nova of KIC 4378554 and V516 Lyr can be naturally understood as an effect of a lower q in V585 Lyr. Since the growth rate of the eccentric mode is proportional to q^2 (Lubow 1991), a typical $q = 0.10$ for the short period V585 Lyr requires ~ 3 times longer time than in a case of $q = 0.18$ in V516 Lyr. Since it took ~ 2 –3 d to reach the maximum amplitude in V516 Lyr and the background dwarf nova of KIC 4378554, the agreement with this expectation is very good and reinforces the TTI theory.

5.2. Period Variation of Superhumps

5.2.1. Global Variation

We studied the period variation of superhumps in all three SU UMa stars by using the $O - C$ data. We did not use period finding methods such as Fourier transform or PDM because the $O - C$ data are more sensitive for detecting the period variation and this method gives a more stable result when the sampling rate is very low. The results are shown in the third panel of figures 1 [which is an improvement of Barclay et al. (2012)], 7, and 15. We note, however, there appeared some wiggles in V585 Lyr, which should not be considered as real since the LC sampling rate in this object was almost exactly one third of the superhump period, which resulted in artificial signals. All three objects show a global decrease in the superhump period (shown by a broken line in the figures): from 0.0778 d to 0.0765 d in the background dwarf nova of KIC 4378554, from 0.0613 d to 0.0600 d in V585 Lyr and from 0.0895 d to 0.0870 d in V516 Lyr. The global decrease in the superhump period during superoutburst in these three stars are thought to be produced by monotonic decrease in the disk radius (Osaki, Kato 2013b).

Among them, V516 Lyr has a photometric orbital period (P_{orb}) and we can determine the precession rate of the eccentric mode (the superhump mode) in the accretion disk. As discussed in Osaki, Kato (2013b), it is very convenient to introduce the fractional superhump deficiency in the frequency unit $\epsilon^* \equiv (\nu_{\text{orb}} - \nu_{\text{SH}})/\nu_{\text{orb}} = 1 - P_{\text{orb}}/P_{\text{SH}}$ where ν_{orb} and ν_{SH} are orbital and superhump frequencies, respectively. The ordinary superhump period excess, $\epsilon \equiv (P_{\text{SH}} - P_{\text{orb}})/P_{\text{orb}}$ is related to this quantity by $\epsilon^* = \epsilon/(1 + \epsilon)$. The quantity, ϵ_+^* , is then related to the apsidal precession rate of the eccentric disk, ν_{prec} , by $\epsilon_+^* = \nu_{\text{prec}}/\nu_{\text{orb}}$. The quantity ϵ_+^* in the growing stage of positive superhumps is thought to reflect the precession

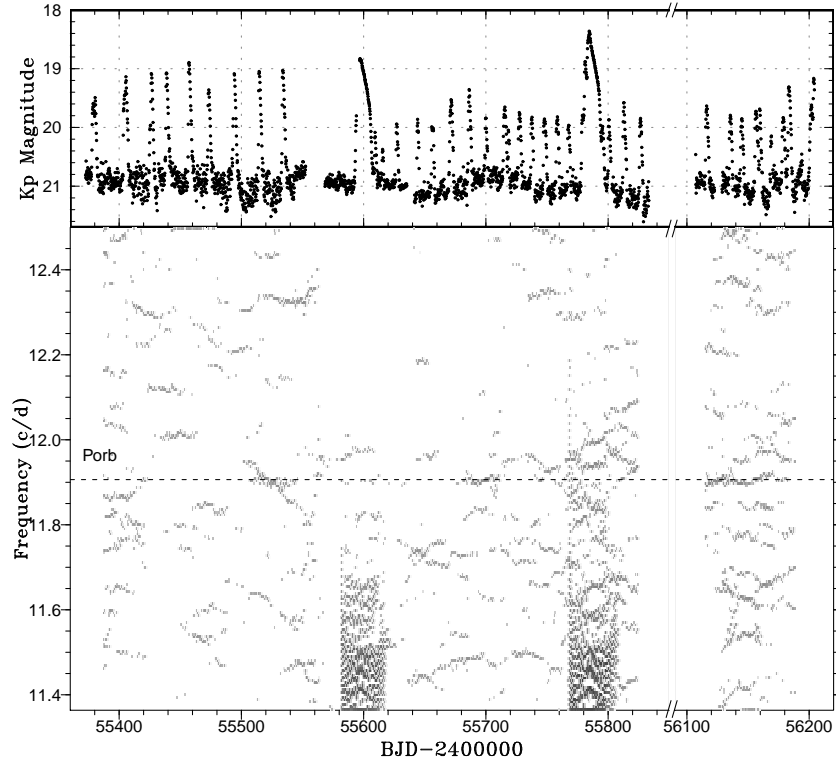


Fig. 17. Two-dimensional Lasso power spectrum of the Kepler LC light curve of V516 Lyr. (Upper:) Light curve; the Kepler data were binned to 0.02 d. Since there is no stable long-term zero point in the Kepler data, we artificially added a constant to the flux of each quarter to obtain the similar level (mag ~ 21) in quiescence. (Lower:) Lasso power spectrum ($\log \lambda = -5.75$). The width of the moving window and the time step used are 30 d and 1 d, respectively.

rate at the 3:1 resonance, because the superhump wave is restricted to the resonance region (Osaki, Kato 2013b). The precession rate in this condition can be expressed as (Hirose, Osaki 1990; Hirose, Osaki 1993):

$$\epsilon_+^* = \frac{\nu_{\text{prec}}}{\nu_{\text{orb}}} = \frac{q}{\sqrt{1+q}} \left[\frac{1}{2} \frac{1}{\sqrt{r}} \frac{d}{dr} \left(r^2 \frac{dB_0}{dr} \right) \right], \quad (1)$$

where r is the radius from the white dwarf primary (in unit of the binary separation). B_0 is written as

$$B_0(r) = b_{1/2}^{(0)}/2 = \frac{2}{\pi} \int_0^{\pi/2} \frac{d\phi}{\sqrt{1-r^2 \sin^2 \phi}}, \quad (2)$$

which is the Laplace coefficient of the order 0 in celestial mechanics (Smart 1953). Using $\epsilon^* = 0.060(4)$ for stage A1 superhumps, we obtained a mass ratio of $q = 0.18(2)$ for V516 Lyr where we used the radius of the 3:1 resonance by $r_{3:1} = 3^{(-2/3)}(1+q)^{-1/3}$.

The global decrease in the superhump periods and hence in the quantity ϵ^* indicates that the disk radius decreased during superoutbursts in these three SU UMa stars. The ϵ^* around the end of the plateau phase of V516 Lyr was 3.4%. This value corresponds to a radius of $0.36A$ if we ignore the pressure effects, where A is the binary separation.

5.2.2. Pressure Effects

As discussed in Osaki, Kato (2013b), we consider that the temporary deviation from the general trend of the period variation is caused by the pressure effects. The

pressure effects bring about a decrease in the superhump eigenfrequency (Hirose, Osaki 1993) and thus a decrease in the (positive) superhump period (Osaki, Kato 2013b), besides the effect of disk radius variation. We interpret that the temporary deviation from the general trend (temporary decrease in period) commonly seen in three systems was caused by the pressure effects. Although the strength of this effect seems to be different from object to object, the effect is the strongest around the early phase of the superoutburst, particularly around the stage A–B transition. This is because the disk temperature is the highest near the start of the superoutburst.

A much stronger downward deviation seen in V585 Lyr in a period of BJD 2455235–2455239, may be understood as a stronger pressure effect. As discussed in Osaki, Kato (2013b), the precession rate of the eccentric mode is given by two different terms of the dynamical prograde precession by the tidal perturbation of the secondary star and of the retrograde precession by pressure effects. V585 Lyr is thought to have a lowest q among the three SU UMa stars discussed here judging from their superhump periods. The pressure effects may affect the precession frequency of the eccentric mode (and the superhump period) more strongly in a low- q system such as V585 Lyr. This is because the prograde precession rate by the tidal effect is lower in a lower- q system while the pressure effects work for retrograde precession similarly regardless of q . Thus the relative importance of pressure effects may increase if

we go to a system of lower q .

5.2.3. Period after Superoutburst

After the superoutburst, the period tends to remain at a short value, probably reflecting a smaller disk radius. It looks like that the period increased around the re-brightening in the background dwarf nova of KIC 4378554 and V585 Lyr which may reflect the increase in the disk radius due to the thermal instability (cf. Osaki, Kato 2013b). The periods of the superhump around this time, however, may not be very reliable because the amplitudes of superhumps were very low. The period variation around the time of “mini-rebrightenings” of V585 Lyr was not very informative due to the noisy $O - C$ diagram and the time-resolution was insufficient to resolve “mini-rebrightenings”.

5.3. Superoutburst without a Precursor

The outburst of V585 Lyr recorded with Kepler did not show a precursor outburst. This is currently the only known superoutburst without a precursor in the Kepler data. In the framework of the thermal-tidal instability model (Osaki 2005), this superoutburst can be understood as follows: if the mass is sufficiently accumulated in the accretion disk during a long quiescence, the next normal outburst could bring the disk to expand to the tidal truncation radius, by passing the 3:1 resonance. The expansion of the disk is stopped at this radius and the disk is then in fully hot state, and the viscous depletion of matter ensues even when the eccentric tidal instability has not yet developed. This allows the disk to develop a growth of eccentric structure (and thus superhumps) a few days after the outburst maximum. This situation corresponds to “case B” superoutburst discussed in Osaki, Meyer (2003) and Osaki (2005).

As shown by Kryachko (2001), V585 Lyr also showed a superoutburst with a precursor [“case A” in Osaki, Meyer (2003)]. This indicates that the properties of V585 Lyr are not so extreme as WZ Sge-type dwarf novae, which predominantly show superoutbursts without precursor and very rarely² show a precursor-superoutburst-type outburst. [For a recent review of WZ Sge-type dwarf novae, see Kato et al. 2001; Kato et al. 2009]. The Kepler data clearly demonstrate that the same object can show two types of superoutbursts, with or without a precursor.

5.4. Late-Stage Superhumps

It has been well known that the prototypical Kepler SU UMa-type dwarf novae V344 Lyr and V1504 Cyg showed the development of secondary humps which evolved into the strongest signal after the fading from the superout-

burst (Wood et al. 2011). This picture agrees with the traditional interpretation of the late superhumps (Vogt 1983), i.e. the varying energy release on an eccentric disk around the stream impact point. The degree of the development of the secondary hump is, however, reported to be different between V344 Lyr and V1504 Cyg, and the latter has much less prominent secondary humps (Kato et al. 2012).

In the present study, none of three objects showed neither a strong sign of the secondary hump nor a ~ 0.5 phase jump expected for traditional late superhumps. This result seems to confirm the ground-based results (Kato et al. 2009; Kato et al. 2010; Kato et al. 2012; Kato et al. 2013) that most of SU UMa-type dwarf novae, particularly low- \dot{M} ones, do not show a ~ 0.5 phase jump characteristic to traditional late superhumps. From the low amplitudes of post-superoutburst superhumps in the three objects, we may conclude that there was no evidence of enhanced mass transfer during the superoutburst.

It appears that V344 Lyr is rather exceptional in its strength of the secondary hump. This may be related to its high \dot{M} as inferred from its short supercycle.

The present result for V585 Lyr clearly confirms that so-called stage C superhumps survive after the fading from the superoutburst without showing a ~ 0.5 phase jump. This has demonstrated our suggestion that at least some “late superhumps” (supposing a ~ 0.5 phase jump) can be understood as a result of mistaken cycle count for stage C superhumps with a shorter period (Kato et al. 2009).

6. Conclusion

We studied Kepler SC and LC light curves of three SU UMa-type dwarf novae: the background dwarf nova of KIC 4378554, V585 Lyr, and V516 Lyr.

Both the background dwarf nova of KIC 4378554 and V516 Lyr showed a similar combination of precursor-main superoutburst, during which superhumps always started to appear in the fading branch of the precursor (the “type A” superoutburst in Osaki, Meyer 2003 and Osaki 2005). This behavior is common to V344 Lyr and V1504 Cyg and strongly supports the TTI theory for the origin of the superoutburst.

V585 Lyr is a borderline object between SU UMa-type dwarf novae and WZ Sge-type dwarf novae. The Kepler LC data recorded one superoutburst without a precursor. The development of this outburst can be understood within the TTI model as a case in which the disk with mass sufficiently accumulated first expanded to reach the tidal truncation radius by a triggering normal outburst and then the tidal instability and the superhump developed after the maximum (the “case B” in Osaki, Meyer 2003 and Osaki 2005). The subsequent development of the $O - C$ diagram perfectly confirmed the existence of three distinct stages (A–B–C) for short- P_{orb} SU UMa-type dwarf novae inferred from ground-based observations. This observation made the first clear Kepler detection of the positive period derivative commonly seen in the stage B superhumps in such dwarf novae. There

² Richter (1992) reported a possible dip in the early stage of the outburst of DV Dra in 1991. The object underwent a superoutburst in 2005 (Kato et al. 2009) and its property was that of a WZ Sge-type dwarf nova ($P_{\text{orb}}=0.0588$ d). V585 Lyr and DV Dra may be similar objects. Recently, a dwarf nova with a very large outburst amplitude (~ 8 mag), OT J075418.7+381225 = CSS130131:075419+381225, showed a precursor outburst (vsnet-alert 15438). This object has a long superhump period of 0.07194 d (vsnet-alert 15438) and may be different from an ordinary WZ Sge-type dwarf nova.

were recurring “mini-rebrightenings” between the super-outburst and the rebrightening.

V516 Lyr is an SU UMa star similar to V344 Lyr but the frequencies of both normal outburst and superoutburst are lower than those of V344 Lyr, which suggests its lower mass-transfer rate than that of V344 Lyr. One of the most interesting aspects in the Kepler light curve of V516 Lyr is the appearance of double outbursts. In the double outburst, the preceding outburst is of the inside-out nature while the following outburst is of the outside-in nature. The double outbursts tend to occur in groups. We have determined the orbital period of V516 Lyr to be 0.083999(8) d. One of superoutbursts of V516 Lyr was preceded by a double precursor. The preceding precursor failed to trigger a superoutburst and the following precursor triggered a superoutburst by developing positive superhumps. There were possible negative superhumps in the LC data of V516 Lyr. One occasion with an appearance of possible negative superhumps coincided with that of a reduced number of normal outbursts, strengthening the conclusion for V1504 Cyg and V344 Lyr (Osaki, Kato 2013a; Osaki, Kato 2013b) that the negative superhumps tend to suppress normal outbursts.

None of these three SU UMa-type showed the strong signature of a transition to the dominating stream impact-type component of superhumps. This finding suggests that the case of V344 Lyr is rather exceptional, which is probably associated with a high \dot{M} . There was no strong indication of enhanced mass-transfer following the super-outburst.

We have also developed a method to analyze superhumps of short- P_{SH} SU UMa-type dwarf novae in the Kepler LC data by modeling the observation and applying the MCMC method. Since most of the new dwarf novae included in the Kepler field by chance (cf. Barclay et al. 2012) are expected to be observed only with LC runs, and a large fraction of dwarf novae is expected to be short- P_{SH} systems (Gänsicke et al. 2009), our method will be effective in characterizing these dwarf novae.

This work was supported by the Grant-in-Aid for the Global COE Program “The Next Generation of Physics, Spun from Universality and Emergence” from the Ministry of Education, Culture, Sports, Science and Technology (MEXT) of Japan. We thank the Kepler Mission team and the data calibration engineers for making Kepler data available to the public.

Appendix 1. Method to Handle Kepler Pixel Image Data with R

Barclay et al. (2012) introduced PyKE routines to extract custom apertures. We introduce a different convenient way: by using FITSio package of R, and loading the target pixel FITS file in a variable `d`, one can easily obtain a time-series data for pixel and draw pixel light curves as in figure 2 in Barclay et al. (2012) and make custom-aperture photometry without a special library. To load a FITS pixel data, we can use the following command (the

file name was split due to its long length; it should be written in a single line in actual execution):

```
library(FITSio)
d <- readFITS("kplr004378554-2009350155506
_lpd-targ.fits")
```

The resultant `d$col` contains the table values in the FITS file. The counts for individual pixel number `n` are stored in `d$col[[5]][,n]`, where 5 means the fifth member of the FITS data (pixel counts). For example, we can draw a light curve for pixel `n=3` by:

```
plot(d$col[[5]][,3])
```

If one wish to add three pixels `n=3, 4, 8`, we can get the summed values by:

```
f <- d$col[[5]][,3] + d$col[[5]][,4] +
d$col[[5]][,8]
```

and

```
plot(f)
```

to draw the light curve for the custom aperture.

Appendix 2. Reconstruction of the Superhump Profile using Kepler LC Data

Since the Kepler LC data were too sparse for a short-period object like V585 Lyr (only three measurements in one superhump), we modeled the observation from the template superhump light curve and obtained the best model referring to the actual observations (subsection 3.2).

In reconstructing the superhump profile, we subdivided observations to 0.5 d segments (~ 24 observations). They were first subtracted for the longer trends caused by outbursts, and the mean residuals were adjusted to be zero. We assumed a template light curve consisting of 20 phase bins. We can then model the observation by numerically integrating the spline-interpolated template for the phases corresponding to each Kepler LC exposure (29.4 min) assuming the epoch and period. We can get from the assumed template a set of $\{y_{\text{model}}(i)\}$, where i represents the Kepler LC exposure. We then compare $\{y_{\text{model}}(i)\}$ with the actual observations $\{y_{\text{obs}}(i)\}$. In principle, we can minimize the difference between $\{y_{\text{model}}(i)\}$ and $\{y_{\text{obs}}(i)\}$ by changing the assumed template. The best-fit model, however, gives a highly structured light curve not resembling that of a superhump. This was probably caused by the “overexpression” of the random or systematic variations other than the superhump variation.

We therefore estimated the best superhump profile by using both the residuals and smoothness using the Bayesian framework. The values $\theta(j)$ ($j = 1, \dots, N$), where N is the number of phase bins, represent the template light curve. The notation follows the appendix of Kato et al. (2010). Since Bayes’ theorem gives

$$Pr(\theta|D) \propto Pr(D|\theta)\pi(\theta), \quad (\text{A1})$$

where θ is the model parameter (in the present case, the template light curve) and D is the observation. $Pr(D|\theta)$ is the likelihood and $\pi(\theta)$ is the prior. $L^0 = \log\{Pr(D|\theta)\pi(\theta)\}$ can be expressed as a form of:

$$L^0 = L_{\text{res}}^0 + \lambda L_{\text{sm}}^0. \quad (\text{A2})$$

Here,

$$L_{\text{res}}^0 = \sum_i \left[-\log(\sqrt{2\pi}\sigma) - \frac{\{y_{\text{obs}}(i) - y_{\text{model}}(i)\}^2}{2\sigma^2} \right], \quad (\text{A3})$$

where σ is the observation error. Following a standard technique in Bayesian analysis, we then express the condition of smoothness of θ by introducing a prior function assuming that second order differences of $\{\theta(j)\}$ follow a normal distribution. Then,

$$L_{\text{sm}}^0 = \sum_j \left[-\log(\sqrt{2\pi}\sigma_s) - \frac{\{\theta(j-1) - 2\theta(j) + \theta(j+1)\}^2}{2\sigma_s^2} \right], \quad (\text{A4})$$

where $\theta(0) = \theta(N-1)$ and $\theta(N+1) = \theta(1)$ reflecting the cyclic condition. σ_s is the standard deviation of the normal distribution. Since only the difference of L^0 is important in the MCMC steps, we can omit constant terms. Since σ and σ_s are constants, we can now write in a form

$$L = \frac{1}{2\sigma^2}(L_1 + L_2) \quad (\text{A5})$$

$$L_1 = -\sum_i \{y_{\text{obs}}(i) - y_{\text{model}}(i)\}^2 \quad (\text{A6})$$

$$L_2 = -\lambda' \sum_j \{\theta(j-1) - 2\theta(j) + \theta(j+1)\}^2, \quad (\text{A7})$$

and $\lambda' = \lambda(\sigma/\sigma_s)^2$. In actual calculation, we estimated the contribution of L_1 and L_2 to L , and expressed $\beta = L_2/L_1$ as the strength of the prior. We changed β and selected the most likely template light curve.

By using the actual Kepler data and after comparison with the superhump light curve taken from the ground-based observation, we adopted $\beta = 0.1$ (for example, $\beta = 1$ gives too smooth, and $\beta = 0.01$ gives too structured light curve compared to the ground-based observation; figure 18). The result, however, does not very strongly depend on β . Since all of the LC measurements of V585 Lyr have more than 7×10^5 electrons, the photon noise is not the dominant source of the error. We therefore used $\sigma = 0.001$ mag for this analysis. The resultant profile, however, is not sensitive to this value.

The probability density function (PDF) of model parameters from the observed data can be determined by MCMC method (cf. Kato et al. 2010), and we adopted the mean and the standard deviation for each phase of the PDF to obtain the template light curve. Note that the standard deviation is not the actual error of the estimate, but only a measure of residuals which is strongly affected by the condition set by the prior. A length of 20000 MCMC run was sufficient to obtain a reasonable PDF and the initial burn-in period was 5000.

We should note this kind of reverse estimation may be prone to artificial features, although the solution in the present case was mostly stable.

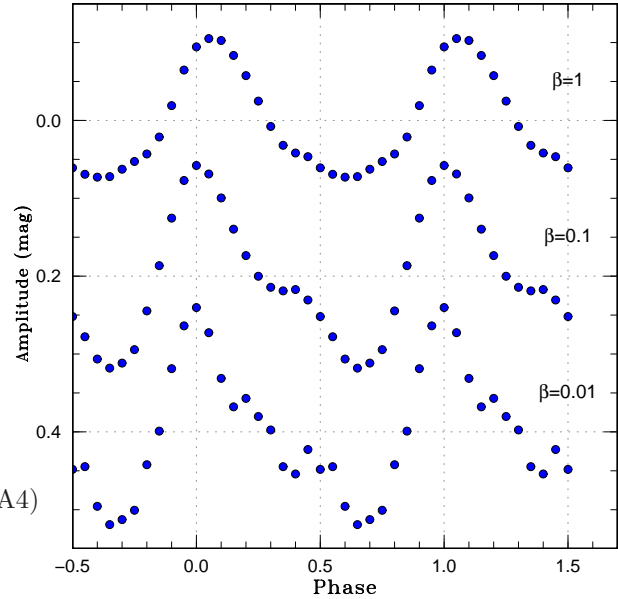


Fig. 18. Dependence on β in reconstructing the superhump profile from the Kepler LC data. The data are for V585 Lyr, 0.5-d segment starting on BJD 2455235 (near the peak amplitude).

Appendix 3. Determination of Superhump Maxima in Kepler LC Data

In subsection 3.3, we determined the times of superhump maxima by using the MCMC method. As in subsection 2, we modeled the observation by using a template with 20 phase bins. In this case, we used the template superhump light curve obtained in appendix 2. Because the superhump profiles varied with time, we averaged the template superhump profiles ± 1 d of the observations. Since the superhump profile was not well determined for stage A, we used the template for BJD 2455236 before this epoch. For the same reason, we used the template for BJD 2455245 after this epoch. The template was normalized to have full amplitudes of 0.2 mag and the zero mean value. The phase of the maximum (determined by spline interpolation) was shifted to phase zero. The definition of the superhump maximum in the present case refers to the light maximum, and is slightly different from Kato et al. (2009), which more reflected the moment of the variation. This difference, however, was very subtle and did not affect the overall $O-C$ appearance.

We used observations in ± 1.5 superhump cycles around the superhump maximum to be measured. These three superhump cycles typically contains 9 observations. We then used a parameter set of {time of maximum, amplitude} to model the observation. The modeling was the same as in appendix 2 and used numerical integration for the spline-interpolated template superhump light curve. Using the likelihood function equation (A3) (no prior was used here), we can perform the MCMC calculation to determine the PDF for the parameter set. We adopted the means and standard deviations of the MCMC results (af-

ter removing the burn-in period) as the mean values and 1σ errors for the estimated time of superhump maximum and amplitude.

References

- Barclay, T., Still, M., Jenkins, J. M., Howell, S. B., & Roettenbacher, R. M. 2012, *MNRAS*, 422, 1219
- Borucki, W. J., et al. 2010, *Science*, 327, 977
- Cannizzo, J. K. 1993, in *Accretion Disks In Compact Stellar Systems*, ed. J. C. Wheeler (Singapore: World Scientific Publishing), p. 6
- Cannizzo, J. K., Smale, A. P., Wood, M. A., Still, M. D., & Howell, S. B. 2012, *ApJ*, 747, 117
- Cannizzo, J. K., Still, M. D., Howell, S. B., Wood, M. A., & Smale, A. P. 2010, *ApJ*, 725, 1393
- Coyne, R., et al. 2012, *MNRAS*, submitted (arXiv astro-ph/1206.6762)
- Fontaine, G., et al. 2011, *ApJ*, 726, 92
- Gänsicke, B. T., et al. 2009, *MNRAS*, 397, 2170
- Garnavich, P., Still, M., & Barclay, T. 2011, *Astron. Telegram*, 3507
- Hirose, M., & Osaki, Y. 1990, *PASJ*, 42, 135
- Hirose, M., & Osaki, Y. 1993, *PASJ*, 45, 595
- Howell, S. B., et al. 2013, *AJ*, 145, 109
- Ichikawa, S., & Osaki, Y. 1994, in *Theory of Accretion Disks-2*, ed. W. J. Duschl, J. Frank, F. Meyer, E. Meyer-Hofmeister, & W. M. Tscharnutter (Dordrecht: Kluwer Academic Publishers), p. 169
- Imada, A., et al. 2009, *PASJ*, 61, L17
- Imada, A., et al. 2008, *PASJ*, 60, 1151
- Ishioaka, R., et al. 2001, *PASJ*, 53, 905
- Kaluzny, J., & Rucinski, S. M. 1995, *A&AS*, 114, 1
- Kaluzny, J., Stanek, K. Z., Garnavich, P. M., & Challis, P. 1997, *ApJ*, 491, 153
- Kaluzny, J., & Udalski, A. 1992, *Acta Astron.*, 42, 29
- Kato, T. 1995, *IBVS*, 4152
- Kato, T. 1997, *PASJ*, 49, 583
- Kato, T., et al. 2013, *PASJ*, 65, 23
- Kato, T., et al. 2009, *PASJ*, 61, S395
- Kato, T., & Maehara, H. 2013, *PASJ*, in press (arXiv astro-ph/1303.1237)
- Kato, T., et al. 2012, *PASJ*, 64, 21
- Kato, T., et al. 2010, *PASJ*, 62, 1525
- Kato, T., Nogami, D., Baba, H., & Matsumoto, K. 1998, in *ASP Conf. Ser. 137, Wild Stars in the Old West*, ed. S. Howell, E. Kuulkers, & C. Woodward (San Francisco: ASP), p. 9
- Kato, T., Nogami, D., Moilanen, M., & Yamaoka, H. 2003, *PASJ*, 55, 989
- Kato, T., Sekine, Y., & Hirata, R. 2001, *PASJ*, 53, 1191
- Kato, T., & Uemura, M. 2012, *PASJ*, 64, 122
- Koch, D. G., et al. 2010, *ApJL*, 713, L79
- Kryachko, T. V. 2001, *IBVS*, 5058
- Lasota, J.-P. 2001, *New Astron. Rev.*, 45, 449
- Lubow, S. H. 1991, *ApJ*, 381, 259
- Meyer, F., & Meyer-Hofmeister, E. 1981, *A&A*, 104, L10
- Mochejska, B. J., Stanek, K. Z., & Kaluzny, J. 2003, *AJ*, 125, 3175
- Ohshima, T., et al. 2012, *PASJ*, 64, L3
- Ohshima, T., et al. 2011, *PASJ*, submitted
- Osaki, Y. 1974, *PASJ*, 26, 429
- Osaki, Y. 1989, *PASJ*, 41, 1005
- Osaki, Y. 1996, *PASP*, 108, 39
- Osaki, Y. 2005, *Proc. Japan Acad. Ser. B*, 81, 291
- Osaki, Y., & Kato, T. 2013a, *PASJ*, in press (arXiv astro-ph/1212.1516)
- Osaki, Y., & Kato, T. 2013b, *PASJ*, submitted
- Osaki, Y., & Meyer, F. 2003, *A&A*, 401, 325
- Osaki, Y., & Meyer, F. 2004, *A&A*, 428, L17
- Patterson, J., et al. 2002, *PASP*, 114, 721
- Ramsay, G., Cannizzo, J. K., Howell, S. B., Wood, M. A., Still, M., Barclay, T., & Smale, A. 2012, *MNRAS*, 425, 1479
- Richter, G. A. 1992, in *ASP Conf. Ser. 29, Viña del Mar Workshop on Cataclysmic Variable Stars*, ed. N. Vogt (San Francisco: ASP), p. 12
- Scaringi, S., Körding, E., Uttley, P., Groot, P. J., Knigge, C., Still, M., & Jonker, P. 2012a, *MNRAS*, 427, 3396
- Scaringi, S., Körding, E., Uttley, P., Knigge, C., Groot, P. J., & Still, M. 2012b, *MNRAS*, 421, 2854
- Shears, J. H., Gaensicke, B. T., Brady, S., Dubovsky, P., Miller, I., & Staels, B. 2011, *New Astron.*, 16, 311
- Smak, J. 1984, *Acta Astron.*, 34, 161
- Smak, J. 2004, *Acta Astron.*, 54, 221
- Smak, J. 2008, *Acta Astron.*, 58, 55
- Smak, J. I. 1991, *Acta Astron.*, 41, 269
- Smart, W. M. 1953, *Celestial Mechanics* (Longmans: London, New York)
- Soejima, Y., et al. 2009, *PASJ*, 61, 659
- Stellingwerf, R. F. 1978, *ApJ*, 224, 953
- Still, M., Howell, S. B., Wood, M. A., Cannizzo, J. K., & Smale, A. P. 2010, *ApJL*, 717, L113
- Uemura, M., et al. 2005, *A&A*, 432, 261
- van der Woerd, H., & van Paradijs, J. 1987, *MNRAS*, 224, 271
- Viallet, M., & Hameury, J.-M. 2007, *A&A*, 475, 597
- Viallet, M., & Hameury, J.-M. 2008, *A&A*, 489, 699
- Vogt, N. 1983, *A&A*, 118, 95
- Warner, B. 1995, *Cataclysmic Variable Stars* (Cambridge: Cambridge University Press)
- Whitehurst, R. 1988, *MNRAS*, 232, 35
- Wood, M. A., Still, M. D., Howell, S. B., Cannizzo, J. K., & Smale, A. P. 2011, *ApJ*, 741, 105
- Zemko, P., Kato, T., & Shugarov, S. 2013, *PASJ*, in press (arXiv astro-ph/1212.5940)